NASA
Technical
Paper
2748

1987

Evaluation of a Scale-Model Experiment To Investigate Long-Range Acoustic Propagation

Tony L. Parrott,
Gerry L. McAninch,
and Ingrid A. Carlberg

Langley Research Center
Hampton, Virginia

National Aeronautics
and Space Administration

Scientific and Technical
Information Division

Summary

Tests were conducted to evaluate the feasibility of using a scale-model experiment situated in an anechoic facility to investigate long-range sound propagation over ground terrain. At a nominal scale factor of 100:1, attenuations along a linear array of six microphones colinear with a continuous-wave type of source were measured over a wavelength range from 10 to 160 for a nominal test frequency of 10 kHz. Grazing-incidence angles ranged from 0° for both sound source and microphones set flush to about 15° for maximum source and microphone elevations and for minimum propagation range. Most tests were made for a hard model surface (plywood), but limited tests were also made for a soft model surface (plywood with felt).

For grazing-incidence propagation over the hard surface, measured and predicted attenuation trends were consistent for microphone locations out to between 40 and 80 wavelengths. Beyond 80 wavelengths, however, significant variability was observed between test runs. A contributing factor to the run-to-run variability at the more remote microphones was the relatively long term disturbances in the propagation medium caused by natural ventilation of the anechoic facility. There was also some evidence of extraneous propagation-path contributions to data irregularities at the more remote microphones.

An analytical model-sensitivity study at the highest test frequency of 12.5 kHz indicated that same-direction systematic errors on the order of ±1 mm in both source and microphone elevations could generate up to 2.5-dB shifts in "relative" excess attenuation trends. For equal elevation errors in opposite directions, however, a cancellation effect apparently occurred that reduced the sensitivity by about 50 percent. For the soft surface, no comparable sensitivity was found.

The results of this study suggest that for an experimental arrangement consisting of a continuous-wave pointlike source, the source and microphone elevations above a hard-surface model should be accurate to within at least ±0.5 mm for a nominal test frequency of 10 kHz. Also, careful attention should be given to source design to ensure that extraneous radiation is at least 40 dB below that from the source radiation orifice. If these conditions are satisfied, then the experiments of the type described in this report should prove fruitful for validating analytical models for predicting long-range propagation over ground terrain, provided that surface impedance can be appropriately modeled.

Introduction

Reliable estimates of sound attenuation for near-grazing-incidence propagation to a surface are required for a number of applications. Since high-frequency acoustic disturbances suffer the greatest atmospheric attenuation, surface-induced losses are of importance primarily for lower frequencies. Because of the numerous physical effects that must be taken into account, theoretical prediction is a challenging problem. Over the past two decades, numerous investigators have contributed to the development of mathematical models for near-grazing-incidence propagation. A thorough review of this work is given by Pao et al. in reference 1. The analyses by Rudnick and Ingard (refs. 2 and 3, respectively) provided the first fundamental consideration of sound radiating from a pointlike source in the vicinity of an infinite plane of finite impedance. In 1975 Chien and Soroka (ref. 4) extended the analysis to include all boundary impedances likely to be encountered. Thus, the analytical development for a point source radiating above a plane boundary with locally reacting impedance appears to be complete at the present time.

Further development to account for the effect of surface irregularities on sound propagation over terrain at low grazing angles has been pursued by several investigators. A summary of this work, given by Howe in reference 5, calculated the effect of a random distribution of small-scale surface irregularities consisting of cylindrical or hemispherical bosses. Howe showed that the net effect is the production of surface waves that are effective in penetrating the ground shadow zone predicted for a smooth surface of the same "effective" impedance. The effect of large-scale surface features with finite impedance boundaries such as ridges and hills is currently being studied by Pierce et al. (See refs. 6, 7, and 8.) The refraction of sound by time-invariant mean velocity and sound speed gradients has been considered in previous studies (see ref. 9) and in a recent textbook (see ref. 10).

All these mathematical models have been developed for idealized terrain geometries, temperature and wind gradients, and ground impedances. It is practically impossible to perform a parametric validation of these models on the basis of measurements conducted in complicated terrain geometries and meteorological conditions actually encountered outdoors. One way to circumvent this difficulty is to develop scale-model experiments that will allow controlled, systematic variations of the most important geometric and physical parameters. Such experiments could validate current simplified models and

provide the basis for further refinements appropriate for full-scale outdoor application.

In reference 11, Hutchins et al. conducted propagation experiments on a 1:80 scale model with a sound source operating over the frequency range from 8 to 100 kHz. Hard asphalt surfaces were modeled with sheet aluminum. Institutional grass was modeled by expanded polystyrene that was sanded and covered with a single layer of tissue paper. The main thrust of this work was to use model results directly to predict full-scale excess attenuations. Generally, good correlations were observed between model and full-scale interference frequencies.

Other scale-model investigations to determine wind and terrain effects on long-range sound propagation have been conducted in special wind-tunnel facilities for studying atmospheric boundary-layer effects. One such work, reported by Tachibana and Yoshihisa in reference 12, used discrete frequencies ranging from 12.5 to 100 kHz to study propagation over scale-model distances of about 1.8 m. By heating or cooling the model surface they were able to separate the effects of thermal and wind gradients near the model surface. Their results were qualitatively consistent with those observed in field investigations. Another investigation reported by Anderson et al. in reference 13 made use of a spark source to study propagation over model surfaces. The unique advantage of their facility was control of wind velocity and boundary-layer characteristics.

Two model ground surfaces were examined in this experiment. One model, designed to simulate a hard asphalt surface, consisted of a 1.6-mm-thick aluminum plate installed on a turntable arrangement in the test-section floor of the tunnel. The other model surface, which simulated grassland, consisted of 2.5-cm-thick extruded polystyrene with light tissue paper glued to the surface. The tunnel test-section dimensions were 2.4 m wide by 1.82 m high by 18.2 m long. The hard reflecting walls required a pulse-type source with appropriate data editing to remove unwanted reflections. The pulse source was driven by an electrical discharge and was characterized by relatively high peak pressure, run-to-run variability, and a continuous spectrum dominated by frequencies ranging from 10 to 50 kHz. Although a pulse-type source will improve signal-to-noise ratios, special care is required to account for source nonlinearity, run-to-run variability, atmospheric absorption, and transducer directionality associated with the high-frequency content of the pulse spectrum. The authors of reference 13 claim to have adequately accounted for these factors in their data acquisition and analysis procedure.

The results of reference 13 were stated as insertion loss of the model surface (excess attenuation) in 1/3-octave bands and for a fixed microphone location of 2.2 m from the source with angles of grazing incidence ranging from 0.7° to about 8°. For the most part, the theory predicted the general trends for propagation over hard and soft flat surfaces with no wind. The authors note that the theoretical doubling of pressure at a hard plane surface was not consistently achieved at low frequencies. In the deep minima associated with destructive interference, measured levels were higher than predicted levels by as much as 20 dB for the hard surface but by only 4 dB for the soft surface. The large discrepancy for the hard surface was attributed to microphone directivity variations and system noise. Also, theory overpredicted the constructive interference maxima by as much as 4 dB for both the hard and soft surfaces. When a model hill with and without wind was tested, the results were far less satisfactory. In this case the theory did not predict any details of the measured surface insertion losses.

In summary, the authors of reference 13 suggested that the results were encouraging. They further suggested that some of the discrepancy between theory and experiment could be due to bending waves induced in the aluminum plate and to directionality characteristics of the microphones. Clearly, the discrepancies between theory and experiment for the simple flat surface under a homogeneous stationary medium should be thoroughly understood and eliminated before proceeding to models that include surface irregularities.

This paper reports the results of an experiment designed to gain a better understanding of environmental control requirements for scale-model simulation of long-range sound propagation over ground terrain at small grazing-incidence angles. Specifically, tests were conducted on a 50-m^2 expanse of model surface located inside an anechoic chamber to minimize reflections. A discrete-frequency (10 kHz) continuous-wave sound was radiated from a pointlike source whose elevation above the model surface could range from 0 to about 2 wavelengths. Two different model-surface impedance conditions were used in this experiment. The baseline surface consisted of high-quality marine plywood to simulate a relatively hard surface condition. A soft-surface condition was simulated with a 3-mm-thick felt covering that was spread over the plywood surface. An existing data acquisition system was used to acquire attenuation data along a linear array of microphones colinear with the source. Synchronous signal averaging was used to improve signal-to-noise ratios for the relatively small, and therefore insensitive, microphones. The

microphone elevations ranged from 0 to about 1.5 wavelengths above the surface. From these measurements, attenuation characteristics of the surfaces were determined. Comparisons of measured and calculated "relative" excess attenuation trends were obtained based on estimated values of the model-surface reflection factors. Finally, recommendations are given based on the experience gained during this study to improve scale-model experiments further for long-range-propagation model validation.

Symbols and Abbreviations

Values are usually given in SI units and, where considered useful, also in U.S. Customary Units.

A_e	excess attenuation
$(A_{e,\text{calc}})_{r_1}$	calculated excess attenuation at r_1 relative to that at reference location $r_{1,\text{ref}}$
$(A_{e,\text{meas}})_{r_1}$	measured excess attenuation at r_1 relative to that at reference location $r_{1,\text{ref}}$
A_f	free-field source strength
A_s	source strength in presence of model surface
A/D	analog-to-digital converter
c	sound speed
D	range from source to microphone receiver
DVM	digital voltmeter
dB/dd	decibels per distance doubling
erfc	complex error function
$F(w)$	boundary-loss factor
FFT	Fast Fourier Transform
f	frequency
H_r	elevation of microphone receiver
H_s	source elevation
h_{rel}	relative humidity, percent
i	$=\sqrt{-1}$
k_1	free-space (atmosphere) wavenumber, ω/c
k_2	wavenumber in model medium
Mic	microphone
P_{ref}	reference sound pressure level
$(P_s)_{r_1}$	acoustic pressure at field point in presence of surface
P_{test}	test sound pressure level
p_b	barometric pressure, mm Hg
Q	image source strength
R	normal-incidence reflection factor
R_p	plane wave reflection coefficient
R_1	model-medium flow resistivity
r_1	path length from source to microphone receiver
r_2	path length from image to microphone receiver
SPL	sound pressure level, dB
ΔSPL	change in sound pressure level, dB
T_a	ambient temperature, °C
T_i	inside temperature, °C
TTL	terminated transmission line
V	outdoor windspeed, knots
w	numerical distance parameter
α	attenuation constant
β	normal-incidence admittance
θ	acoustic resistance
ξ	normal-incidence impedance
ξ_c	characteristic impedance of model medium
ρ	density of air
τ	propagation constant of model medium
ϕ	grazing-incidence angle

χ	acoustic reactance
ψ	angular locations of circular-arc microphones relative to radial-array microphones, deg
ω	angular frequency

Subscripts:

calc	calculated
ref	reference

Experimental Setup and Procedure

General Description

The design of a scale-model, long-range propagation experiment requires compromises in the available space, ambient environment control, source power and radiation characteristics, microphone sensitivity and size, and data acquisition and analysis system. This experiment was exploratory in nature and did not permit the design and development of the most desirable source and microphone characteristics. In particular, source power, stability, and mechanical isolation from the model surface were marginal. Also, microphone sensitivity was compromised for small size to minimize directionality effects. It was anticipated at the beginning of the design phase that these compromises could be compensated for to some extent by means of an existing sophisticated data acquisition and analysis procedure.

The design and layout of the experimental setup is shown in the plan view diagram of figure 1. The microphone locations are represented by the open circles with distances from the source (shaded symbol) shown in wavelengths (λ) at the nominal test frequency of 10 kHz. The experimental objective was to simulate long-range sound propagation over a model surface between a point source and microphone arrays at low, audible frequencies. This simulation was done by means of a scale-model arrangement that trades off a reduction in geometric dimensions for an increase in frequency. Thus, $k_1 D$ remains constant, where k_1 is the free-space wavenumber and D is the propagation range. To avoid contaminating reflections, the model surface was required to be effectively infinite and bounded by a nonreflecting enclosure. This was accomplished by installing the model surface on the floor of the Langley Anechoic Noise Facility and by providing curved shrouds along the surface boundaries to minimize edge diffraction.

Realistic modeling of ground impedance requires that the model-surface impedance be equal to that of the full-scale surface over the frequency range of interest. It is unrealistic to expect available materials to exhibit the same impedance over the test frequency range of interest as that of specific ground surfaces ranging from vegetation-covered soil to concrete. In this initial experiment, impedance modeling was a secondary consideration. The model-surface choices were 19-mm-thick (3/4-in.), high-quality marine plywood and the same surface covered with 3-mm-thick (1/8-in.) felt.

A radial and circular-arc array of microphones centered on the source location was positioned as indicated in figure 1. The radial microphones were spaced at successive distance-doubling points with the first microphone located about 10 wavelengths from the source, based on a nominal test frequency of 10 kHz. This frequency choice approximated a model/full-scale dimension ratio of 1:100. Five circular-arc microphones 120 wavelengths from the source were installed nominally 18° apart (symmetrically located with respect to the linear array). The purpose of the circular-arc array was to monitor potentially troublesome behavior attributable to source directivity, model-surface vibration, and residual-edge diffraction or reflections. To encourage desynchronization in residual-edge-diffracted wave arrival times, the radial array was skewed with respect to the surface diagonal (i.e., 23.4° with respect to the longer surface edge). Note that microphone 5 serves as both a radial and a circular-arc receiver.

The model surface was assembled from 15 modules, each with dimensions 1.2 m by 2.4 m (4 ft by 8 ft), as indicated in the sketch of figure 2(a). Each module consisted of a continuous sheet of marine plywood attached to a wood support structure around its periphery. The modules were supported in the anechoic chamber by evenly spaced, steel rails running parallel to the concrete floor that normally support sections of a "false" plywood floor about 0.3 m above the concrete floor of the facility. The total elevation of the model surface was about 0.6 m above the concrete floor or 22.2 cm (8.75 in.) above the few remaining sections of the false plywood floor. This installation allowed sufficient access space for source driver, microphone preamplifiers, and cabling. Assembly of the complete model surface was conducted by one-at-a-time placement of the modules on the support rails. Gaps between adjacent modules were filled with epoxy-based filler that was sanded flush with the module surfaces. Upon each placement, shims were used to achieve an elevation as nearly equal as possible to the previously installed modules by use of a carpenter's bubble level. In this

manner, point-to-point slope changes, over the length of the level (1.22 m), were maintained to within $\pm 0.3°$. Upon completion, the structure could support the weight of test personnel, an important consideration because it was necessary to change the source and microphone elevations manually. Lateral compression forces on the entire assembly were supplied by a series of tensioning cables strung through the module supports.

As previously mentioned, the model-surface periphery was terminated by a curved shroud to minimize contamination by edge-diffracted waves. The details of this structure are illustrated in figure 2(b). The critical feature of the shroud design was the smooth transition from the flat surface to the curved surface with minimum surface discontinuity. The radius of curvature, 20.3 cm (8.0 in.), was large relative to the longest wavelength of interest (i.e., 3.8 cm at 9 kHz). Past experience with such shrouds, reported in reference 14, indicated that contamination from edge-diffracted waves was minimized by this technique.

The source consisted of a high-frequency audio tweeter (5 to 15 kHz) available at audio supply outlets. The tweeter was modified and attached to a brass tube (with an outside diameter of 1.9 cm and an inside diameter of 0.64 cm) by means of an adapter section as illustrated in the sketch of figure 3. The inside diameter of the brass tube was such that only plane wave propagation could be supported up to about 15 kHz, the upper frequency limit of the driver. Plane wave propagation through the tube ensured cylindrically symmetric radiation from the source. The 10-cm length of the brass tube allowed a maximum source elevation of 5.8 cm. For zero source and microphone elevations, this source arrangement was capable of generating 76 to 95 dB over the frequency range from 9 to 13 kHz at the reference microphone location. Thus, an SPL range from about 52 to 71 dB would be expected at the most distant microphone location for a hard surface.

The microphones used were 3-mm-diameter (1/8-in.) condenser microphones. The standard adapters furnished by the manufacturer to connect the microphones to their respective preamplifiers allowed a maximum elevation of 3.6 cm above the model surface without the larger diameter preamplifier section protruding into the sound field. In the standard configuration recommended by the manufacturer, the lower limit of the dynamic range of the microphone and preamplifier system is 76 dB. The signal level at the most distant microphone location was estimated to range from 50 to 55 dB for zero source and microphone elevations. Time-domain synchronous averaging was expected to extend the lower limit of the dynamic range to provide the additional signal-to-noise ratio needed at the more distant microphones.

To permit the easy removal of both the sound source and the microphones, circular sections or plugs of plywood were machined to fit snugly into the appropriate cutouts of the model surface. (See fig. 4.) The undersides of the mounting plugs were equipped with a cam and locking arrangement to allow a mechanically hard connection to the model surface. To remove the assembly for calibration and maintenance, a special spanner-type wrench was designed to disengage the cam mechanism, thereby permitting the assemblies to be lifted from their seated positions. During test operations, the source driver was embedded in a mass of modeling clay (about 2 kg (1 lb)) to reduce source driver radiation into the access space underneath the model surface. Despite the added mass, measurements with the source removed from the model surface indicated a decrease of only about 20 dB in the SPL upon plugging the source radiation orifice. Although this level of extraneous radiation from the source driver was of some concern, it was anticipated that the model surface would shield the "test space" from the undesired radiation since the driver would be located underneath the model surface.

Calibration Apparatus

Figure 5 is a schematic diagram of the apparatus for performing frequency response comparisons of the microphone measurement systems. The device consisted of a 5 mm by 1 mm rectangular waveguide running through the center of a rectangular aluminum block. The size of the waveguide ensured that only plane acoustic waves were transmitted at frequencies below about 20 kHz. A reference microphone and a measurement microphone were mounted flush on the waveguide walls opposite each other. The waveguide was then connected to a sound source at one end, and the exit end was terminated in a length of tubing to reduce end reflections inside the channel. In this manner, comparison frequency responses of all microphone systems could be obtained over a time period of about 1 hr. These calibrations, repeated at intervals during the tests, were used to evaluate the overall repeatability of the data acquistion and analysis system. An absolute calibration was performed for all the microphones using a commercially available calibrator operating at 1.0 kHz.

Data Acquisition and Analysis

The on-line data acquisition and analysis system used in this experiment was an adaptation of that developed for the source monitoring system of the spinning mode synthesizer in the Langley Aircraft

Noise Reduction Laboratory as described in reference 15. The instrumentation layout is shown schematically in figure 6. For a given test frequency, source input current and sound pressure measurement systems were under direct computer control, as indicated by the instruments marked by an asterisk. Upon establishing an acceptable source level, the sound field at the microphone locations was sampled in a systematic manner by switching the multiplexer under computer control. Microphone signals were conditioned by the autogain amplifier and 50-Hz-bandwidth tracking filter to provide optimum input to the A/D converter. The maximum sampling rate of the A/D converter was 40 kHz which permitted about 2.7 samples per cycle at a frequency of 15 kHz. Source driver stability was monitored by performing a measurement at the reference microphone each time that a measurement was completed at a more distant microphone. (That is, sound pressure levels were measured in the sequence: Mic 1, Mic 2, Mic 1, Mic 3, ..., etc.) An FFT analyzer was used to monitor broadband spectra from microphone system outputs as indicated in the instrumentation schematic diagram.

Time-domain, synchronous averaging reduces the contribution of incoherent noise in proportion to $N^{1/2}$, where N is the number of averages. Thus, the low-end dynamic range of a measurement system can theoretically be improved indefinitely. However, there are practical limits on the time available for the process. In this experiment, a sufficient amount of synchronous averaging was done to provide an effective signal enhancement of about 20 dB.

To accomplish signal enhancements of up to 20 dB, 200 blocks of pressure time history data, each consisting of 160 data points, were phase synchronized to a common time origin and then averaged. For a nominal test frequency of 10 kHz, this procedure allowed up to 7200 cycles of the fundamental waveform to be processed for each set of 200 data blocks. From the stored "averaged digitized wave form," the amplitude and phase of a sinusoidal least squares fit were calculated. The stored calibration factors were then applied to calculate the SPL and phase. The above procedure was repeated five times, and then the resulting five SPL's and phases were averaged to obtain a final value for a given microphone location.

Because of direct or natural ventilation of the anechoic facility, temperature and relative humidity were not controlled. Thus, temperature and relative humidity tended to correlate with outdoor meteorological conditions. These parameters were recorded by sensors located on one wall of the facility. Absolute accuracies for the temperature and relative humidity readings were not greater than 1°C and 1 percent, respectively.

Analysis

Propagation Model

As an aid to evaluating the scale-model propagation experiment described in this paper, relative trends of the measured and computed excess attenuation are compared. The computations are based on the analysis of a point source radiating in the presence of a finite impedance surface of infinite spatial extent. The simplified formulation given by Chessell (see ref. 16) was deemed adequate since, for the parameter range of interest in this investigation, the surface wave is insignificant.

Figure 7 depicts the relevant source and microphone geometry for a point source near an infinite plane. The upper region represents the atmosphere; the lower region, the model medium. The source and microphone elevations are taken as H_s and H_r, respectively; the grazing-incidence angle is ϕ and the range is D. The distances from the source and image to the microphone are denoted by r_1 and r_2, respectively. The wavenumber of the disturbance is k_1 in the atmosphere and k_2 in the model medium. Atmospheric absorption is neglected but the possibility of extended reaction of the model medium is included. For discrete-frequency emission from a point source, the pressure $(P_s)_{r_1}$ at the microphone consists of the superposition of the contributions from the direct and reflected fields. Thus, the total pressure at r_1, with the temporal dependence suppressed for convenience, is given by

$$(P_s)_{r_1} = \frac{A_s}{r_1} \exp(ik_1 r_1) + \frac{Q}{r_2} \exp(ik_1 r_2) \quad (1)$$

Here, A_s is the source strength and Q is an effective image source strength, where

$$Q = R_p + F(w)\,(1 - R_p) \quad (2)$$

Note that Q is defined in terms of the plane wave reflection coefficient R_p and the so-called boundary-loss factor $F(w)$. For surfaces characterized by extended reaction, i.e., internal wave motion parallel to the surface, the plane wave reflection coefficient for a medium with an effectively infinite depth is

$$R_p = \frac{\sin\,\phi - \beta\left[1 - (k_1/k_2)^2\,\cos^2\phi\right]^{1/2}}{\sin\,\phi + \beta\left[1 - (k_1/k_2)^2\,\cos^2\phi\right]^{1/2}} \quad (3)$$

which, for a locally reacting surface, reduces to

$$R_p = \frac{\sin\ \phi - \beta}{\sin\ \phi + \beta} \tag{4}$$

More elementary analyses replace the image source strength Q with the plane wave reflection coefficient R_p. However, for grazing incidence, $\phi = 0°$ and $r_1 = r_2$. Consequently, $R_p = -1$ regardless of the value of β. Thus, the elementary analyses predict the complete absence of an acoustic field for $\phi = 0°$. The boundary-loss factor $F(w)$ is a function of the numerical distance w which for an extended reacting surface is given by

$$w = \frac{2ik_1r_2\beta^2}{(1-R_p)^2\ \cos^2\phi}\left(1 - \frac{k_1^2\ \cos^2\phi}{k_2^2}\right) \tag{5}$$

and for a locally reacting surface becomes

$$w = \frac{1}{2}ik_1r_2\frac{(\sin\ \phi + \beta)^2}{1 + \beta\sin\ \phi} \tag{6}$$

The boundary-loss factor describes phenomena in the vicinity of the impedance boundary associated with spherical wave propagation at near-grazing-incidence angles. When k_1r_2 is small or β is small (or both), $F(w) \approx 1$ and $Q \approx 1$, independent of R_p, thus resolving the anomaly that results when R_p is naively used in place of Q in equation (1). For the other limiting cases, i.e., with high frequencies, longer ranges, and larger surface admittances, then $w >> 1$ and $F(w) \approx 0$. Equation (2) then reduces to the familiar plane wave result. Chessell calculates $F(w)$ from an asymptotic series good for absolute values of w less than 1 or greater than 10 and neatly avoids the range of $|w|$ between 1 and 10 over which the current experiment takes place. Therefore, it was necessary to evaluate $F(w)$ directly using a result from Chien and Soroka (ref. 4) as follows:

$$F(w) = 1 + i\sqrt{\pi w}\ \exp(-w)\ \mathrm{erfc}\left(-i\sqrt{w}\right) \tag{7}$$

For later application it will be convenient to write equation (1) with the direct-wave contribution isolated as follows:

$$(P_s)_{r_1} = A_s\frac{\exp(ik_1r_1)}{r_1}\left\{1 + \frac{r_1}{r_2}Q\ \exp\left[ik_1(r_2 - r_1)\right]\right\} \tag{8}$$

The bulk of current experience suggests that acoustic propagation over real soil surfaces can be adequately described by analytical models incorporating the locally reacting assumption. However, for the model surface consisting of felt on plywood, significant extended reaction effects may exist.

A comparison of equations (3) and (4) suggests that extended reaction can alter the incidence angle at which R_p changes sign for certain critical combinations of the incidence angle and surface admittance. For maximum source and microphone elevations, the grazing-incidence angles in this experiment ranged from about 0.6° at the most distant microphone to about 10° for the nearest microphone. Because of the possible sign change in reflection coefficient at the more distant microphone locations, an effort was made to estimate β as well as k_2 at the test frequencies of interest. These estimates, over the test frequency range from 9.0 to 13.0 kHz, were obtained with the aid of impedance measurements over a limited frequency range from 0.5 to 3.0 kHz. In addition, flow resistance measurements were obtained for the felt covering. These measurements were used with a semiempirical model for porous materials developed by Delany and Bazley (see ref. 17) to provide the desired estimates of β and k_2 over the test frequency range. This procedure will be discussed further in the "Results and Discussion" section.

Procedure for Correlating Experiment With Theory

Excess attenuation at a point r_1 in the presence of a surface is defined as an insertion loss of the surface expressed in decibels relative to the free-field pressure at the same point. In the literature, it is generally assumed that the source strength and directivity are invariant for a change in the radiation environment. If the source strength should change because of the presence of the surface, the "apparent" excess attenuation follows from equation (2) as

$$A_e = 20\log\left(\frac{A_s}{A_f}\right) + 20\log\left|1 + \frac{r_1}{r_2}Q\exp\left[ik_1(r_2 - r_1)\right]\right| \tag{9}$$

where A_f is the free-field source strength. For $A_s = A_f$ (i.e., no change in source strength due to the surface), the first term is zero and the result would reduce to the "true" excess attenuation because of ground effects alone.

In the present experiment, not only did $A_s \neq A_f$ but also A_s changed slowly with time because of acoustic driver degradation. It was therefore inconvenient to compare experiment and theory directly on the basis of equation (9), which implies a knowledge of the ratio A_s/A_f. Instead, measured and calculated relative excess attenuations were compared. This procedure will now be described.

A knowledge of A_s alone would allow the sound pressure level at a point r_1 to be calculated from equation (1) as follows:

$$(\mathrm{SPL_{calc}})_{r_1} = 20\log\left[\frac{|(P_s)_{r_1}|}{P_{\mathrm{ref}}}\right] = 20\log\left(\frac{1}{r_1}\frac{A_s}{P_{\mathrm{ref}}}\right)|1 + (r_1/r_2)Q\,\exp[ik_1(r_2 - r_1)]| \quad (10)$$

where P_{ref} is the reference sound pressure level (20 μPa). The source strength A_s can be estimated via equation (10) by inserting measured values of $(\mathrm{SPL})_{r_1}$ at a reference location $r_{1,\mathrm{ref}}$. Thus, a relative excess attenuation at any other field point can be calculated; i.e.,

$$\left(A_{e,\mathrm{calc}}\right)_{r_1} = (\mathrm{SPL_{calc}})_{r_1} - 20\log\left(\frac{1}{r_{1,\mathrm{ref}}}\frac{A_s}{P_{\mathrm{ref}}}\right) - 20\log\left|1 + \frac{r_{1,\mathrm{ref}}}{r_{2,\mathrm{ref}}}Q\exp\left[ik_1(r_{2,\mathrm{ref}} - r_{1,\mathrm{ref}})\right]\right| \quad (11)$$

Measured relative excess attenuations can be compared with the calculated values from equation (11) by performing the following operation on the measured sound pressure levels:

$$(A_{e,\mathrm{meas}})_{r_1} = (\mathrm{SPL_{meas}})_{r_1} - (\mathrm{SPL})_{r_{1,\mathrm{ref}}} - 20\log\left(\frac{r_{1,\mathrm{ref}}}{r_1}\right) \quad (12)$$

It should be noted that both the calculated and measured relative excess attenuations as given by equations (11) and (12) will be zero at the reference location. In the experiment, this condition is actually achieved by normalizing the experimental and calculated values to zero at microphone 1, a procedure which effectively accomplishes the same result as formally solving equation (10) for the source strength A_s. Clearly, this procedure allows only measured and calculated trends of excess attenuation to be compared. However, for this particular experiment, the difference between calculated and measured relative excess attenuations is indicative of inadequacies in the analytical model and/or sensitivity to systematic errors in measured parameters.

Results and Discussion

Comparisons of Microphone Frequency Response

Comparisons of the system frequency response which includes source control, data acquisition, and microphone measurement systems were made during the tests. In figure 8 the results of five representative comparison responses, obtained with the specially constructed calibration device described previously, are presented. The tests were conducted during a time period of several days to provide an indication of system stability.

The response comparisons are presented in figure 8 for the six microphone systems used in the radial-array measurements. The data were obtained using the same computer-controlled source and data acquisition system used in the scale-model experimental setup. Responses of each microphone channel are presented for five different dates as indicated in the figure key. The key also includes ambient temperature, relative humidity, and barometric pressure. The responses were measured at frequency increments of 1.0 kHz and ranged from 9.0 to 13.0 kHz.

With two exceptions, the maximum variability among the six microphone systems, as defined by the dashed parallel lines, ranged from 0.6 dB for microphones 4 and 5 to 0.8 dB for microphone 1. At 12 kHz, the responses for microphones 1 and 2 ranged up to 1 dB. When such excursions occurred, they were scrutinized as possibly being indicative of equipment malfunction.

The conclusion drawn from this exercise is that the system response, including microphone system and data acquisition system, was invariant with respect to both time and frequency to within about 0.8 dB. Thus, 0.8 dB sets a lower limit below which the variability associated with sound propagation over the model surface may be difficult to resolve. Also, 20-Hz-bandwidth spectra of the background noise obtained with an FFT analyzer, as seen by the microphones installed on the model surface, indicated levels from 52 to 54 dB over the test frequency range. For a perfectly reflecting surface, a pure tone level of 80 dB would be required at microphone 1 to produce a level of 56 dB at microphone 6, the most distant microphone. Synchronous signal averaging was expected to provide at least 20-dB improvement in the signal-to-noise ratio at the most distant microphone.

Measured Model-Surface Impedance

The normal-incidence impedances or, equivalently, the complex reflection factors (see eq. (5) with $\phi = 0°$), for the plywood and felt-covered plywood test specimens were measured. Photographs of two square test specimens ($\approx$5 cm by $\approx$5 cm) are shown in figure 9. These measurements were performed in an impedance tube with the same cross-sectional dimensions as the test specimens. The specimen impedance was determined from the standing wave pattern generated by normally incident and

reflected waves at the test specimen surface. For highly reflecting surfaces with reflection factors above about 0.95 (standing wave ratios of 32 dB or greater), direct measurement of the standing wave parameters is prone to imprecision and inaccuracy because of ambient noise interference with null level measurements. A multipoint sampling technique has been developed at the Langley Research Center that circumvents the need for direct measurements in sharp nulls as required by the standing wave method. The technique essentially allows a reconstruction of the standing wave pattern from a selected number of pressure and phase measurements. The impedance is calculated from the reflection factor obtained from the best fit of a one-dimensional propagation model to the data. Comparisons between reflection factor magnitudes using this method and the standing wave method for highly reflective materials such as steel indicate that the multipoint method can consistently measure reflection factor magnitudes in excess of 0.95 with a repeatability of ± 0.005.

Figure 10 shows the measured normal-incidence impedances (normalized by ρc) plotted against frequency for both model surfaces. (See the figure key for symbol definitions.) For comparison, the measured impedance trend for a soil surface as reported by Embleton et al. in reference 18 is represented by the short-long dashed curves. As might be expected, both impedance components for the hard and soft model surfaces decrease in magnitude with increasing frequency. The soil-surface impedance components have a similar frequency dependence. However, the impedance components for the plywood surface decrease at precipitous rates compared with those for the soil surface, at least up to the maximum measurement frequency of 3.0 kHz. The resistive component, in particular, appears to decrease below the soil resistance mean value at 3.0 kHz. When the felt covering is added, the impedance components are in better agreement with those of the soil surface, especially from about 2.0 to 3.0 kHz.

The challenge of devising a model-surface impedance to appropriately scale a "real" surface at a chosen scale factor is dramatically illustrated by these data. For example, the indicated graphical extrapolations of the plywood-surface data (short dashed curves) suggest that at a scale factor of about 20, the reactance component may be a fair approximation of that of soil at 0.5 kHz as indicated by the shaded areas centered on 0.5 and 10 kHz; however, the resistance component is not well-modeled. In a later section, these impedance data will be used in conjunction with a semiempirical model to extrapolate the model-surface impedance into the test frequency range of interest.

Acoustic Propagation Test Data

In this section, acoustic propagation test results will be presented and discussed. During the course of the experiment, 296 runs were obtained over a time period of about $2\frac{1}{2}$ months. The test configurations consisted of source and microphones all flush, all at maximum elevation, all at one-half elevation, and various combinations of source or microphones flush and the other at one-half or maximum elevation. Test frequencies ranged from 9.0 to 13.0 kHz in 0.5-kHz increments. Most of the runs were conducted for the hard surface with several repeat runs throughout the time period to document test data variability. All the basic data are presented in two formats. Along the radial microphone array, the distribution of sound pressure levels in decibels is plotted versus $\log(k_1 D)$, where D is the range from the source to a particular microphone. Along the radial array, the microphone at location 1 (microphone 1) served as a reference. At the nominal test frequency of 10 kHz, D ranged out to about 160 wavelengths. Along the circular-arc array, the distribution of sound pressure in decibels relative to microphone 5, jointly shared by the radial and circular-arc arrays, is plotted versus angular distance from the radial array.

Run-to-run, random variations of the measured SPL's were observed among the circular-arc microphones and the more distant radial microphones. These variations suggested a combination of extraneous propagation paths and temporal changes in the propagation medium. A more thorough discussion of these factors will be reserved until after presentation of representative data.

To illustrate the data quality, the results of a repetitive sequence of six runs are shown in figures 11 and 12 for frequencies from 10.0 to 12.5 kKz conducted on 2 different days over a 4-hr timespan and for both source and microphones flush with the hard surface. The "a" and "b" parts of each figure show the radial and circular-arc SPL distributions, respectively. On the radial distribution plots, 6-dB/dd reference lines have been superimposed to indicate expected spatial attenuation rate due to spherical spreading for an infinite, perfectly reflecting surface and nonabsorbing medium. In figure 11(a), which shows the radial SPL distributions, there are several features worthy of note. First, source output changes by about 20 dB as the frequency is incremented in 0.5-kHz steps from 10.0 to 12.5 kHz. This is caused mostly by the change in loading on the driver because of resonant behavior of the source adapter. Second, at test frequencies of 12.0 and 12.5 kHz for which the reference levels at microphone 1 exceeded 90 dB, the attenuation rate is measurably greater than 6 dB/dd,

in a consistent pattern, at the more distant microphones. Third, the other test frequencies, whose initial reference levels were less than about 85 dB, tend to exhibit attenuation rates greater than 6 dB/dd, but with significant random variation both within a given run and among runs for the more distant microphones.

Figure 11(b) shows the SPL variation along the circular-arc array. The pressure levels in this figure are plotted in decibels relative to that at microphone 5, which is at the center of the circular-arc array and is shared with the linear array. (See fig. 1.) Angular variation in the sound pressure levels for a given test frequency is seen to be greatest between the $-36°$ and $-18°$ microphone locations, reaching nearly 12 dB for run 1 at the 10-kHz test frequency. With the exception of run 1, the variations for the two positive angular locations were 3 to 5 dB less than those for negative angular locations.

Figure 12 shows a repeat of the test sequence shown in figure 11 but conducted 4 days later. In figure 12(a) the most obvious change compared with figure 11(a) is the 5-dB decrease in reference level of the 12.0-kHz test frequency and the 2-dB increase for the 11.0-kHz test frequency. For the remaining test frequencies, the reference levels are approximately the same as those for the morning runs of figure 11(a). There are, however, changes in levels from 3 to 5 dB at the more remote microphone locations.

A comparison of figure 12(b) with figure 11(b) reveals that the circular-arc variation in sound pressure levels changed significantly between the test dates. At the $-36°$ angular location, all levels changed relative to microphone 5 by up to 14 dB. At other angular locations, especially the positive ones, the changes were not nearly as great. In figure 12(b) the variability at the $-36°$ location was greater than that at the same angular location on the earlier test date, whereas at the other circular-arc locations the variability was generally less than that on the first test date. Figure 12(b) also suggests that the run-to-run variability increased with angular distance from the radial array.

In the remainder of this report, attention will be concentrated on two representative frequencies, 9.0 and 12.5 kHz, near the extremes of the frequency range investigated. The first set of three figures will show "raw" data for the 9.0-kHz test frequency and for several repeat runs. Two source and microphone configurations will be discussed. The first configuration had the source and microphones all at zero elevation above the model surface, and the second configuration had the source at its maximum elevation of 5.84 cm and the microphones all at their maximum elevation of 3.56 cm. Most of the data will be for the hard-surface condition. Limited soft-surface results will be presented for the elevated source and microphones. When the source and microphones were at zero elevation on the soft surface, large attenuation rates precluded adequate signal-to-noise ratios for meaningful results. Following the 9.0-kHz data, the same sequence for the 12.5-kHz data will be presented. Although the circular-arc data were collected for all runs, no further presentations of these data will be made because they exhibited the same variability discussed previously throughout the experiment. Finally, the results will be cast in relative excess attenuation form and correlated with calculations based on the model-surface impedance extrapolations discussed previously.

Figure 13 shows hard-surface radial SPL distributions for four repeat runs at a test frequency of 9.0 kHz and for the source and microphones at zero elevation. The 10-dB change in levels between runs 226 and 229 is due to the replacement of the source driver between those runs. Note in the figure key that these data were taken over a time period of 10 days during which the outdoor windspeed varied by 4 knots, the indoor temperature varied by 2°C, and the indoor relative humidity varied by 9 percent. As was the case for the previous radial distribution data, the levels generally attenuate at a rate greater than 6 dB/dd in a consistent manner through microphone 4. Again, the deviations at microphones 5 and 6 are typical of the data variability observed at the more distant microphones shown in previous figures.

Figure 14 shows the SPL distribution data similar in format to that of figure 13 except for six repeat runs with the source and microphones at maximum elevations. For this configuration, an interference maximum occurs between microphones 1 and 2. Note that these data were taken on the same day and that the temperature varied by about 1°C, typical of morning-to-afternoon changes. The radial SPL's are seen to vary by not more than 1 dB at the various microphone locations, with the exception of microphone 6 which exhibits a 3-dB variation. In general, there was less run-to-run variation for elevated source and microphones.

The behavior of radial SPL distributions for the source and microphones at maximum elevations above the soft surface is illustrated in figure 15 for seven repeat runs. Here, four out of seven runs show relatively good radial SPL distributions. These four runs (270, 273, 276, and 279) were all conducted on the same day ranging from the morning to afternoon during which an air temperature change of about 1°C

was recorded. It is of interest to note that run 285, the last run of the series and conducted on the same day as the other four runs listed above, is in good agreement except at microphones 4, 5, and 6. Also, the outdoor windspeed had been recorded at 13 knots during the previous hour even though it had subsided to 8 knots during the actual run.

Figures 16 to 18 show radial SPL distributions for the 12.5-kHz test frequency in the same sequence and format as in the previous figures for the 9.0-kHz test frequency. These data confirm the same general trends observed for the 9.0-kHz case. Again there was large variability in the circular-arc SPL distributions, which are not shown. As with the 9.0-kHz case, the radial distributions for the hard surface tend to exhibit increased variability at the more remote microphone locations with the source and microphone elevations at zero. For the elevated source and microphone configuration, run-to-run data consistency at the remote microphone locations improves. The addition of a soft surface does not significantly change the data variability for the maximum source and microphone elevation.

Data Variability and Possible Causes

Possible causes of the data variability observed in figures 11 to 18 will now be discussed. The variability can be classified into two categories. First, there was a relatively slow systematic decrease in the output level of the source with time for constant driver voltage (which was always set at the maximum "safe" level). Second, there was random variability observed for the circular-arc array and to a lesser extent at microphones 5 and 6 along the radial array. This random variability observed at microphones 5 and 6 was manifested by deviations from the 6-dB/dd trend at the more distant microphones and the variation at these same microphones in repeat tests.

The time scale for changes in driver output, attributable to driver degradation and to temperature-dependent resonance behavior, was such that the variable driver output was not a problem over a time period of 20 min required for a typical run. Driver degradation over operating time periods of 8 to 16 hr usually mandated driver replacement. The criterion for driver replacement was failure to maintain a level of at least 76 dB at microphone 1 for a test frequency of interest and for zero source and microphone elevations. This criterion was based on an assumed, minimum level of 52 dB at microphone 6. The ambient broadband noise level ranged from 52 to 54 dB as measured by an FFT analyzer set for a 20-Hz bandwidth and connected to the microphone multiplexer output. (See fig. 6.) Synchronous time-domain signal averaging extended the effective system noise floor down to about 20 dB on a unit bandwidth basis.

The random variability was likely associated with time-varying environmental influences on the direct, reflected, as well as extraneous, propagation paths. The time scale for these variations ranged from approximately 1 hr to several days. Thus contamination from competing propagation paths other than those emanating from the source radiation orifice is believed chiefly responsible for observed data variability. This possibility appears to be supported by the results of some diagnostic tests conducted with power applied to the source but with the radiating orifice plugged to reveal "leakage" radiation. Comparisons of level changes at microphones 1 and 6 for unplugged and plugged conditions at 12.5 and 13.0 kHz indicated only a 7-dB level change at microphone 6 for a 24-dB level change at microphone 1. The level changes at microphone 6 were not limited to the broadband noise floor because a spectral peak, with the source orifice plugged, was clearly evident above the background noise floor even without signal enhancement. Inspections conducted at the edge shroud termination near the false facility floor revealed detectable sound propagating in the access space between the model surface and anechoic chamber floor. All these tests were made after a quick remedy was implemented to reduce leakage radiation by embedding the source driver in about 2 kg (1 lb) of modeling clay.

Assuming that such extraneous propagation paths alluded to above were present, then it would appear possible that thermal gradients induced by convection currents or by the normal thermal cycling of the building structure could alter the relative propagation speeds and thus cause time-dependent interference with the desired signals. In addition, time-dependent refraction was possibly induced by thermal gradients near the model surface. Time-dependent refraction can cause signal fluctuations at the distant microphones even in the absence of extraneous propagation paths. Also, residual-edge-diffracted and reflected waves from small hard objects in the anechoic chamber such as light bulbs and electrical conduits may have been contributors to spurious propagation paths. However, a simple scattering calculation for a worst-case situation, consisting of a 25-mm-diameter cylinder placed 1 m from microphone 6, indicated a scattered amplitude at least 20 dB below the incident wave.

To recapitulate, the temporal data variability at the most distant microphones was apparently due to the combined effects of source "leakage" into undesired propagation paths coupled with time-varying convective and refractive effects, driven by

thermal cycling and natural ventilation of the building structure. Marginal signal strength relative to the noise floor of the broadband instrumentation system was not perceived to have been a contributing factor. Although these effects significantly degraded the data quality at the more distant microphone locations, the data from the less distant microphones (i.e., locations 1 through 4) were relatively stable and consistent. Therefore, the overall results were encouraging.

Comparison of Theory With Experiment

In this section, comparisons between experimental and analytical results, as discussed previously in the "Analysis" section, will be presented. Representative results will be discussed for 9.0 and 12.5 kHz, for zero and maximum elevations of source and microphones, and for the hard and soft model surfaces. To help relate the relative excess attenuation results to the radial, absolute SPL's already discussed, intermediate results will be presented in which all levels are referenced to microphone 1. Also, these plots include calculated attenuations based on both hard- and soft-surface reflection factors. Finally, the same results will be shown in terms of measured and calculated relative excess attenuations for various choices of the surface flow resistivity parameter. As indicated in the "Analysis" section, the boundary-loss factor $F(w)$ is a key parameter that describes the spherical wave interaction with the finite impedance boundary condition. In the test frequency range of this experiment, the values of surface impedance needed to evaluate $F(w)$ were extrapolated by a procedure to be described below.

Because it was not possible to measure the model-surface impedance with the available equipment in the test frequency range of interest, it was necessary to extrapolate the measured impedance to these frequencies. To accomplish this extrapolation in a rational manner, an attempt was made to fit the measured data by a semiempirical model produced by Delany and Bazley. (See ref. 17.) This model permits the acoustic properties of a porous medium to be estimated based on measured values of material flow resistivity. For completeness, the equations representing the model are given as follows:

$$\theta = 1 + 0.0571(\rho f/R_1)^{-0.754} \tag{13}$$

$$\chi = -0.087(\rho f/R_1)^{-0.732} \tag{14}$$

$$\alpha = k_1\left[0.189(\rho f/R_1)^{-0.595}\right] \tag{15}$$

$$k_2 = k_1\left[1 + 0.0978(\rho f/R_1)^{-0.700}\right] \tag{16}$$

Equations (13) and (14) give the normalized characteristic resistance θ and reactance χ in terms of the flow resistivity parameter $\rho f/R_1$. Equations (15) and (16) give the attenuation constant α and wavenumber k_2 in terms of the wavenumber for air k_1 and the flow resistivity parameter. The characteristic impedance and propagation constant of the material then become, respectively,

$$\xi_c = \theta + i\chi \tag{17}$$

and

$$\tau = \alpha + ik_2 \tag{18}$$

The normal-incidence impedance of a bulk-reacting material (felt in the present case) of depth l on a highly reflecting surface (plywood) was adapted from a well-known formula for a transmission line terminated in an impedance characterized by a reflection factor R. (See eq. (1.04) in ref. 19 by Zwikker and Kosten.) Making use of the estimated values of ξ_c and τ from equations (17) and (18), respectively, the surface impedance is

$$\xi = \xi_c \frac{[(1+R)\ \cosh(\tau l) + \xi_c(1-R)\ \sinh(\tau l)]}{[(1+R)\ \sinh(\tau l) + \xi_c(1-R)\ \cosh(\tau l)]} \tag{19}$$

from which the surface admittance β is obtained by

$$\beta = 1/\xi \tag{20}$$

Values of β calculated from equations (19) and (20) and values of k_2 taken from equation (16) were used in equation (4) to estimate R_p. Then, R_p and k_2 were used in equation (5) for estimating w. Then, $F(w)$ was calculated from equation (7) and, finally, Q from equation (2). For an extended reacting surface, equations (3) and (5) are used instead of equations (4) and (6) to calculate R_p and w, respectively. Directly measured values of $|R_p|$, obtained in an impedance tube at low frequencies, were compared with calculated values at higher frequencies for both hard and soft model surfaces.

Equations (13) to (20) were applied to the plywood model surface treated as a single layer of infinite depth and to the felt-covered plywood treated as a two-layer medium. The two-layer medium was modeled with the aid of the modified, terminated transmission line (TTL) model as specified by equation (16). A measurement of flow resistance for the felt was obtained by standard means, the results of which are presented in figure 19 for two felt test specimens. The median value for two samples at zero velocity was taken to be as indicated in figure 19.

The plywood terminating surface in the two-layer medium was characterized as being either a perfectly reflecting surface or a reflection factor taken from the extrapolation described above for the uncovered plywood surface.

Figure 20 shows the extrapolated reflection factor magnitude into the test frequency range of interest for the hard and soft model surfaces. For the scope of this study, only the reflection factor magnitude was extrapolated. The normal-incidence reflection factor, as opposed to the impedance, is preferred for this extrapolation because the separate effects of reflection factor magnitude and phase changes have greater physical meaning than a change in the real and imaginary impedance components. Reflection factor magnitude relates to the energy reflected by the surface and therefore to the interference null depths, whereas the phase part tends to control the interference null locations. Because it is unrealistic to expect a scale-model surface to match both impedance components to those of the full-scale surface, it is perhaps more meaningful to make a choice between reflection factor magnitude and phase than between resistance and reactance.

In figure 20 the short-long dashed curve shows the trend of the measured reflection factor magnitude for a soil surface as calculated from the data of reference 18. The real and imaginary parts of the measured impedance are presented in figure 10. This curve is included in figure 20 for reference purposes only. No attempt will be made to match the soil-surface and model-surface reflection factor magnitudes in this experiment. Extrapolations of reflection factor magnitudes for the hard surface were obtained from the semiempirical model (ref. 17) by Delany and Bazley (eqs. (13) and (14)) applied to the hard surface treated as a porous medium of infinite depth. The plot shows the results for three different values of the flow resistivity parameter. Apparently, the measured reflection factors, represented by the square symbols, are best described by a flow resistivity between 20×10^6 and 40×10^6 kg/m^3-sec.

Also in figure 20, calculated reflection factor magnitudes are presented for the soft-surface specimen for two different flow resistivities of the felt. The felt-covering thickness was taken as 3.1 mm (1/8 in.). The reflection factor magnitude for the soft surface did not differ significantly when the plywood reflection factor was changed from 1.0 to the extrapolated values from figure 20. No reasonable value of the flow resistivity, including the possibility of a plywood-surface reflectivity less than 1, allowed the TTL model to describe the measured data (diamond symbols). The TTL model curves are relatively close below 4 kHz but diverge above 4 kHz for the two indicated resistivities. The higher flow resistivity is associated with the lower reflection factor in the high-frequency range.

Another surprising feature of the measured reflection factor magnitude for the hard- and soft-surface specimens is the occurrence of more scatter for the soft-surface reflection factor magnitude. Generally, more scatter would be expected for the higher reflectivity associated with the hard surface. These results indicate that the multipoint sampling method is capable of producing repeatable results at reflectivities approaching 1.0. Thus, it appears that the scatter or variability in the data for the soft-surface specimen is somehow associated with the felt-on-surface composite arrangement. One potential source of variability for such test specimen configurations consisting of contiguous layers of different materials in intimate, but unbonded, mechanical contact is the likelihood of small air spaces or nonuniform mechanical contact at the layer-to-layer interface. (See ref. 20 by Smith and Parrott.) It should be noted that the soft-surface model does not provide an acceptable "scaled impedance" for any known outdoor surface and therefore serves only as a lower limiting value for this scale-model validation experiment.

Figure 21 shows the results of a parametric evaluation of the boundary-loss factor $F(w)$ for a range of the numerical distance parameter w (see eqs. (6) and (7)) likely to be encountered. Only $\log|F(w)|$ versus $|w|$ is shown here for brevity. Referring to equation (2) for the image source strength Q, it will be recalled that when $F(w)$ approaches 1 (i.e., when the surface impedance is high or $k_1 R$ is small), the image strength factor is approximately $+1$ and is independent of the value of R_p. For large $k_1 R$ and smaller surface impedances, $F(w)$ approaches zero and the plane wave result is retrieved. In figure 21 the range of numerical distance for the hard and soft model surfaces is indicated for both flush (zero elevation) and maximum source and microphone elevations. Clearly, this experiment did not explore the entire range of numerical distance; however, representative segments of the low, middle, and high ranges of the numerical distance magnitude were investigated. Also note that increased source and microphone elevation increases the $|w|$ range for the hard surface, whereas for the soft surface the elevation has no significant effect on the range of $|w|$. In figure 21(b) relatively large oscillations occur in $F(w)$ for values of $|w|$ ranging between 5 and 20.

Figure 22 shows the radial-array attenuation data of figure 13 for 9.0 kHz at zero source and microphone elevations. The attenuation is normalized to microphone 1 which, in effect, removes run-to-run

variability from the data. Also on the plot, calculated attenuation curves have been superimposed for a perfectly reflecting surface (i.e., $Q = 1$; see eq. (2)) and for high and low values of flow resistivity obtained from the extrapolations for the plywood surface as shown in figure 20. For this particular case, calculated results for the high value of flow resistivity and a perfectly reflecting surface are essentially the same. For the low value of flow resistivity, the calculated attenuation gradually deviates from the curve for a perfectly reflecting surface to a value about 1.5 dB greater at the most distant microphone. With the exception of microphone 5, the high flow resistivity value correlates with the upper bound of the measured attenuations. The roll-off of the calculated attenuation for the low value of flow resistivity tends to correlate with the tendency of the measured attenuations to roll off from the 6-dB/dd curve at the more remote microphones.

Figure 23 shows the data of figure 22 expressed in the format of relative excess attenuations. The sign convention for excess attenuation chosen here is the same as that used by Chessell in reference 16. Therefore, positive excess attenuation indicates that a sound pressure level at a given microphone is lower than it would be in the presence of a nonabsorbing surface. Essentially, this data presentation format removes the 6 dB/dd and thereby allows the "nonspherical spreading effects" to be studied separately. Thus, in the presence of a perfectly reflecting rigid surface bounded by an inviscid medium, the relative excess attenuation for this configuration would be zero which, from the comparison with the almost perfectly reflecting surface in the previous figure, is approximated by the solid line labeled with a flow resistivity of 80×10^6 kg/m^3-sec. Again, the calculated relative excess attenuation for a surface flow resistivity of 20×10^6 kg/m^3-sec has also been included. Note that the term "relative excess attenuation" means that the calculated and measured values have been forced to agree at microphone 1. This effect produces the same results that would be obtained if the measured SPL at microphone 1 were used to calculate the source strength. Differences between calculated and measured values at other microphone locations indicate inadequacies of the theoretical model, sensitivity to systematic measurement errors, or random scatter due to extraneous noise.

Figure 23 suggests that no reasonable value of surface flow resistivity allows the predictive model to describe the behavior of the measured relative excess attenuation in an average sense. Despite the measured data variability, the general trend of the data suggests significant absorption at zero grazing-incidence angle.

Figures 24 and 25 present the same plot sequence as that in figures 22 and 23 but with the source and microphone elevations at their maximum values. Figure 24 again shows no change in the predicted attenuation between a perfectly reflecting surface and the highest value of plywood flow resistivity of 80×10^6 kg/m^3-sec. Note that the data variability is much less when the source and microphones are elevated. Also, even though the data trend is accurately predicted, the theory is 2 to 3 dB below the data trend. Again, it should be emphasized that perfect agreement at the reference location is forced to occur, which effectively provides the source strength A_s. This procedure causes any positioning error sensitivity at microphone 1 to manifest itself as an "apparent" systematic discrepancy between the calculated and measured results at other locations. This constitutes a disadvantage of this method of comparison. Nevertheless, in the absence of all analytical model inadequacies and systematic measurement errors, the analytical and measured results would agree.

Figure 25 shows the same data in the relative excess attenuation format and with calculated curves for two additional surface flow resistivities as indicated in the figure. Apparently, the data trend correlates slightly better with the intermediate value of flow resistivity. Note also that the data for the elevated source and microphones are on the negative side of the calculated curve in contrast with the zero-elevation source and microphones, in which case the data tended to be on the positive side of the calculated curve. These shifts of the calculated curves with respect to the data again suggest sensitivity to measured parameters used as input to the analytical model. As an example of such sensitivity, the effect of small changes in source and microphone elevations on the calculated relative excess attenuation will be discussed next.

Figure 26 shows the effect on the calculated results when source and microphone elevations are varied from their nominal values of 5.84 and 3.56 cm, respectively. For same-direction elevation changes of about 2.5 mm, the curves shift by 1.5 to 2.5 dB. In fact, positive elevation increments of 2.5 mm for both the source and the microphone bring the predicted behavior into excellent agreement with run 241. Elevation errors for the source and microphones for the hard surface were not greater than about 2 mm. However, small, randomly distributed changes in surface slope up to about $\pm 0.3°$ due to the surface installation procedure could have added significantly to the relative source and microphone elevation error.

Figure 27 shows a comparison to measured and calculated attenuations for the maximum source and

microphone elevations above the soft-surface model. As can be observed, there is a dramatic increase in the attenuation as compared with that for the hard surface. (See fig. 24.) Data for zero elevation above the soft surface were not meaningful because of the rapid attenuation of the acoustic level below the instrumentation plus ambient noise floor. It is of interest to note that the measured attenuations in figure 27 apparently confirm a conservative dynamic range of at least 50 dB in that several attenuations in the neighborhood of 50 dB relative to microphone 1 are obtained. Again, these observations seem to suggest that the instrumentation noise floor may not have been the cause of random variability, but rather contributions from spurious propagation paths. The bracketing values of 30×10^3 and 65×10^3 kg/m^3-sec for the soft-surface flow resistivity (see figs. 19 and 20) generate essentially the same prediction for the attenuation profile. Interestingly, the general trend of the measured attenuations appears to be well-predicted.

Figure 28 shows the same data plotted in the relative excess attenuation format. Although not included in this figure, small changes in the source and microphone elevations had no discernible effect on the calculated results for the soft surface. Again, except for the large data variability, the calculated result appears to describe the average behavior of the data. These results are interesting because they suggest that the agreement between the math model and experiment tends to be less sensitive to microphone-positioning error than is the case for the hard-surface condition, even in the presence of severe contaminating influences.

The final set of five figures (figs. 29 to 33) shows comparisons of measured and predicted relative sound pressure level distributions and relative excess attenuations along the radial microphone array for the test frequency of 12.5 kHz. This frequency is near the upper limit of the frequency range investigated. These figures are presented in the same format as that for the 9.0-kHz data. The results are similar to those for 9.0 kHz and tend to support the same conclusions; consequently, the discussion of these data will be abbreviated.

Radial sound pressures in decibels relative to microphone 1 for six repeat runs at zero source and microphone elevations, taken from figure 16, are shown in figure 29. Superimposed on the data are calculated levels for surfaces characterized by flow resistivities of 20×10^6 and 80×10^6 kg/m^3-sec and by a perfectly reflecting surface ($Q = 1$) as indicated in the figure. As in the 9.0-kHz case, the flow resistivity of 80×10^6 kg/m^3-sec is effectively a perfectly reflecting surface.

As previously noted for the 9.0-kHz test frequency, the data repeatability is reasonably good except for microphone locations 4, 5, and 6 which again exhibit greater variability. Referring to figure 16, three of the runs (227, 230, and 233) were made in the afternoon of the same day but during a time of modest change in outdoor windspeed and temperature. Runs 230 and 233 are in good agreement for all microphone locations except for number 4, for which there is a difference of about 2 dB. Starting at microphone 3, run 227 deviates most widely from the other runs. The remaining runs (207, 224, and 254) were made on different days, and for run 207 the air temperature was about 3°C to 4°C below that for the other runs. As previously noted, there is no problem with the measurement system noise floor for these data because the lowest absolute level is 60 dB, or over 30 dB above the effective measurement system noise floor. These observations provide further support for the possibility that spurious propagation paths were responsible for the variability.

In figure 30 the same data are presented in relative excess attenuation format. Clearly, data variability tends to mask any discernible trends; however, the bulk of the data points fall in the positive region of relative excess attenuation. Thus, as in the corresponding configuration for the 9.0-kHz case (see fig. 23), there is a suggestion that the surface is less than a perfectly reflecting one at grazing incidence.

For the source and microphones at maximum elevations, the attenuations normalized to reference microphone 1 for the hard-surface condition are shown in figure 31. Note that the reference microphone is now well within the first interference null. The outlying data points fall 2 to 5 dB above the nearest calculated curve. Also, note that at this frequency a surface flow resistivity of 80×10^6 kg/m^3-sec generates a result that is quite different from the perfectly reflecting surface ($Q = 1$) and seems to be in better agreement with the data than either the perfectly reflecting surface or the flow resistivity surface of 20×10^6 kg/m^3-sec. This statement is confirmed by figure 32 which shows these same data in the relative excess attenuation format. As with the corresponding plot for the 9.0-kHz data (fig. 25), the data fall on the negative side of the calculated curves.

Figure 33 illustrates the effect of same-direction increments of 0.64 mm (0.023 wavelengths) in source and microphone elevations from the nominal, measured values of 5.842 cm and 3.556 cm for the source and microphones, respectively. This elevation-error magnitude is well within the range expected for this experiment. The figure clearly demonstrates that changes in relative excess attenuation of 2 to 3 dB

can result for same-direction systematic errors on the order of 1 mm at this particular test frequency. However, if the errors are in the opposite direction, i.e., source error positive and microphone error negative, calculations (not shown in the figure) indicate that some cancellation occurs, thus reducing the effect by about 50 percent. The results of figures 26 and 33 suggest that for hard-surface scale models, operating at nominal test frequencies of 12.5 kHz, differences between measured and predicted relative excess attenuation of 1 dB can easily result from source and microphone elevation errors of 0.5 mm.

Because of possible thermal gradients near the model surface that may arise from thermal cycling of the building structure, a calculation was made to determine the relative effects of same-direction elevation errors and a 0.5°C thermal gradient extending 2 cm above the model surface. For maximum source and microphone elevations, such a thermal gradient was found to cause negligible phase shift compared with that due to the same-direction elevation errors of 0.64 mm at a propagation distance of 40 wavelengths.

Concluding Remarks

Tests were conducted to evaluate a scale-model experiment for studying long-range sound propagation at small grazing-incidence angles ranging from 0° to 15°. Both hard- and soft-surface models were tested. The hard surface was achieved with high-quality marine plywood, and the soft surface was achieved by covering the plywood with a layer of 3-mm-thick felt. For a nominal scale-model operating frequency of 10 kHz, a discrete-frequency pointlike source radiated sound over an array of microphones arranged colinearly with the source. Source and microphone elevations ranged within about 2 wavelengths of the model surface. The entire apparatus was located in an anechoic facility. The microphones were positioned at distance-doubling increments from the source, starting at 10 wavelengths and going out to 160 wavelengths.

Numerous repeat runs were performed over a time period of about 2 months to document data consistency for a range of frequencies and combinations of source and microphone elevations. Generally, the data consistency from run to run was good over a propagation range between 40 and 80 wavelengths. Beyond 80 wavelengths, significant variability was evident. Also, variability between runs was generally greater when the source and microphones were at zero elevation, i.e., flush with the model surface. Contributors to the variability may have been residual-edge diffraction, that is, reflections from objects such as light bulbs and time-varying refraction in the propagating medium associated with natural ventilation of the anechoic facility. In addition, extraneous propagation paths arising from the imperfectly isolated source driver located underneath the model surface may have aggravated the variability problem.

General trends of the measured "relative" excess attenuations were in good agreement with predicted trends for the less-distant microphones. Even when significant data variability was present for the more distant microphones, the average trends were predicted by the analytical model. The most critical experimental parameters, as suggested by an analytical model-sensitivity study, were same-direction source and microphone elevation errors. Such errors, which could easily range up to 2.5 mm in this experiment, were shown to result in up to 3-dB shifts in the predicted relative excess attenuation curves for the hard-surface model. When source and microphone elevation errors were in opposite directions, however, a cancellation occurred that reduced the shift by at least 50 percent. For the soft-surface model, such shifts were not predicted.

The results of this study suggest that for sound radiating from a pointlike source over hard-surface models, source and microphone elevation accuracies should be better than ±0.5 mm to limit systematic discrepancies between measured and predicted relative attenuation to about 1 dB for a nominal test frequency of 12.5 kHz. Also, careful attention should be given to source design to ensure that extraneous radiation is at least 40 dB below that from the source radiation orifice. If these conditions are satisfied, then the experiments of the type described in this report should prove fruitful for validating analytical models for predicting long-range propagation over ground terrain, provided that surface impedance can be appropriately modeled.

NASA Langley Research Center
Hampton, Virginia 23665-5225
September 2, 1987

References

1. Pao, S. Paul; Wenzel, Alan R.; and Oncley, Paul B.: *Prediction of Ground Effects on Aircraft Noise.* NASA TP-1104, 1978.
2. Rudnick, Isadore: The Propagation of an Acoustic Wave Along a Boundary. *J. Acoust. Soc. America,* vol. 19, no. 2, Mar. 1947, pp. 348–356.
3. Ingard, Uno: On the Reflection of a Spherical Sound Wave From an Infinite Plane. *J. Acoust. Soc. America,* vol. 23, no. 3, May 1951, pp. 329–335.

4. Chien, C. F.; and Soroka, W. W.: Sound Propagation Along an Impedance Plane. *J. Sound & Vib.*, vol. 43, no. 1, Nov. 8, 1975, pp. 9–20.
5. Howe, M. S.: *On the Long Range Propagation of Sound Over Irregular Terrain.* NASA CR-3862, 1984.
6. Pierce, Allan D.; Main, Geoffrey L.; and Kearns, James A.: Curved Surface Diffraction Theory Derived and Extended Using the Method of Matched Asymptotic Expansions. Paper presented at the Acoustical Society of America Meeting (Cleveland, Ohio), May 1986.
7. Pierce, Allan D.; Main, Geoffrey L.; Kearns, James A.; Benator, Daniel R.; and Parish, James R., Jr.: Sound Propagation Over Large Smooth Ridges in Ground Topography. Paper presented at the International Congress of Acoustics (Toronto, Canada), July 1986.
8. Pierce, Allan D.; Main, Geoffrey L.; Kearns, James A.; and Hsieh, H.-A.: Sound Propagation Over Curved Barriers. *Progress in Noise Control—Inter-Noise 86, Volume I,* Robert Lotz, ed., Noise Control Foundation, c.1986, pp. 495–500.
9. Blokhintsev, D. I.: *Acoustics of a Nonhomogeneous Moving Medium.* NACA TM 1399, 1956.
10. Pierce, Allan D.: *Acoustics—An Introduction to Its Physical Principles and Applications.* McGraw-Hill, Inc., c.1981.
11. Hutchins, D. A.; Jones, H. W.; and Russel, L. T.: Model Studies of Acoustic Propagation Over Finite Impedance Ground. *Acustica*, vol. 52, no. 3, Feb. 1983, pp. 169–178.
12. Tachibana, H.; and Yoshihisa, K.: The Effects of Wind and Temperature Conditions on Outdoor Sound Propagation (Scale Model Experiment). *Noise Control: The International Scene—Inter-Noise 83, Volume 1,* Noise Control Foundation, c.1983, pp. 283–286.
13. Anderson, G. S.; Hayden, R. E.; Thompson, A. R.; and Madden, R.: *Evaluation of the Feasibility of Scale Modeling To Quantify Wind and Terrain Effects of Low-Angle Sound Propagation.* NASA CR-172488, 1985.
14. Willshire, William L., Jr.; and Nystrom, Paul A.: *Investigation of Effects of Microphone Position and Orientation on Near-Ground Noise Measurements.* NASA TP-2004, 1982.
15. Palumbo, Daniel L.: *An Operations Manual for the Spinning Mode Synthesizer in the Langley Aircraft Noise Reduction Laboratory.* NASA CR-165698, 1981.
16. Chessell, C. I.: Propagation of Noise Along a Finite Impedance Boundary. *J. Acoust. Soc. America,* vol. 62, no. 4, Oct. 1977, pp. 825–834.
17. Delany, M. E.; and Bazley, E. N.: *Acoustical Characteristics of Fibrous Absorbent Materials.* NPL Aero Rep. Ac 37, British Natl. Physical Lab., Mar. 1969.
18. Embleton, T. F. W.; Piercy, J. E.; and Olson, N.: Outdoor Sound Propagation Over Ground of Finite Impedance. *J. Acoust. Soc. America,* vol. 59, no. 2, Feb. 1976, pp. 267–277.
19. Zwikker, C.; and Kosten, C. W.: *Sound Absorbing Materials.* Elsevier Publ. Co., Inc., 1949.
20. Smith, Charles D.; and Parrott, Tony L.: Comparison of Three Methods for Measuring Acoustic Properties of Bulk Materials. *J. Acoust. Soc. America,* vol. 74, no. 5, Nov. 1983, pp. 1577–1582.

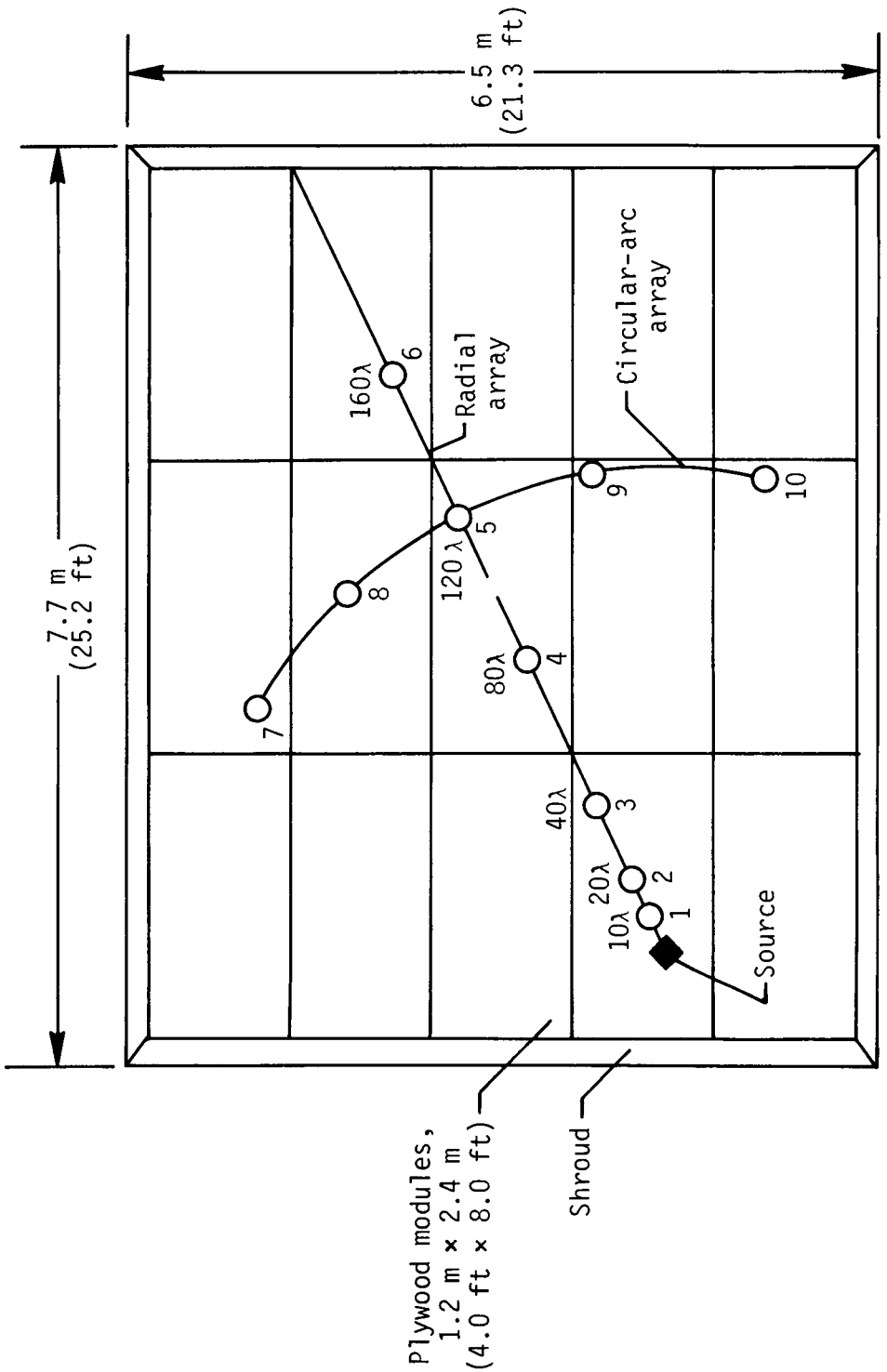

Figure 1. Plan view of scale-model sound propagation experiment showing relative locations of sound source and microphone arrays.

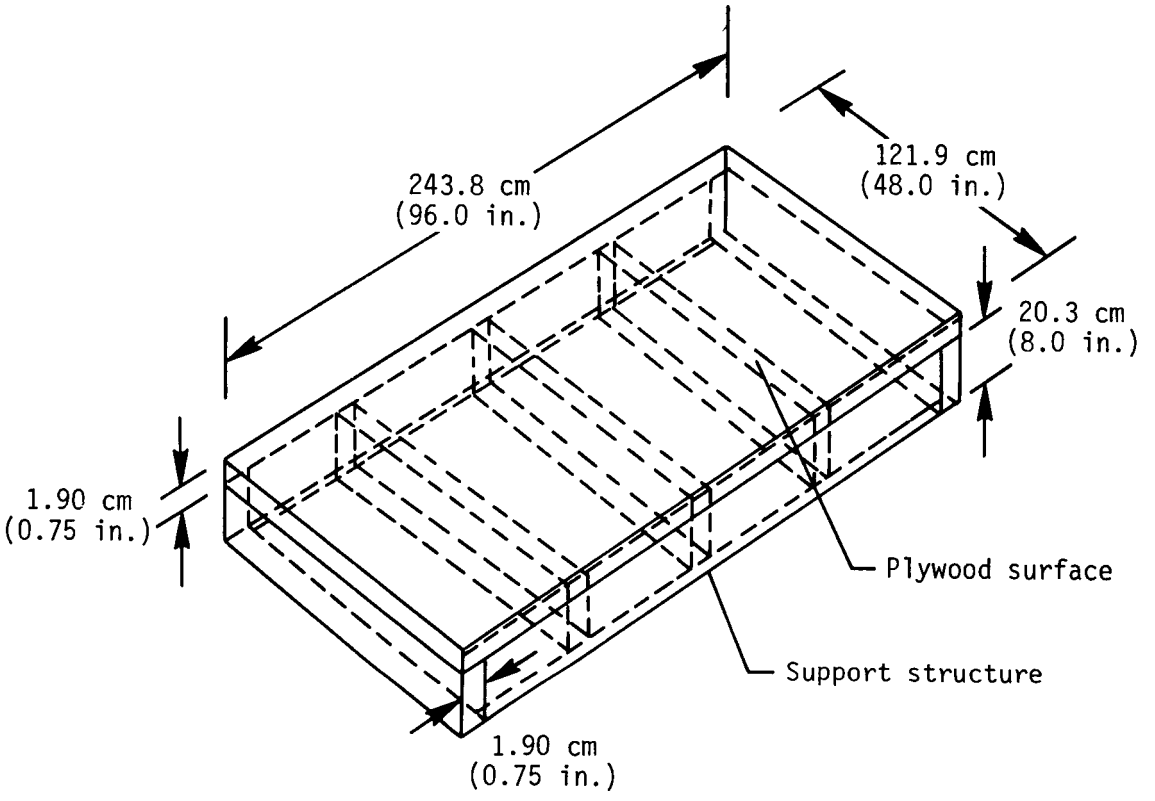

(a) Sketch showing construction of model-surface module.

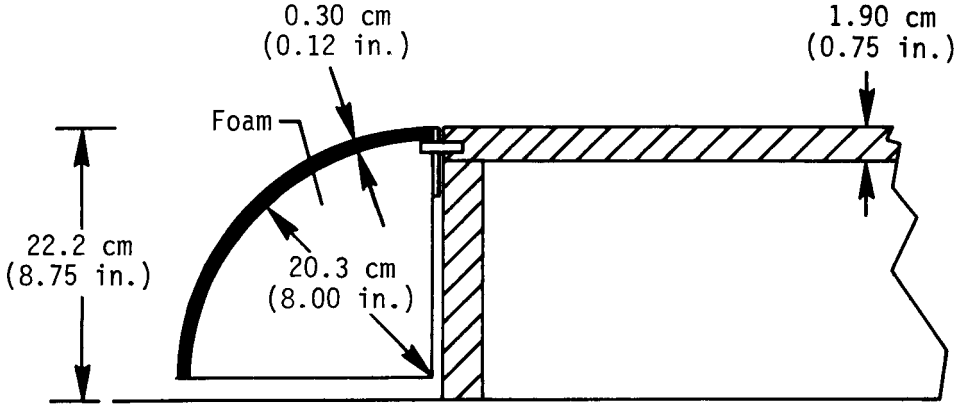

(b) Sketch showing shroud design for minimizing edge-diffraction effects.

Figure 2. Module for model surface (1 of 15).

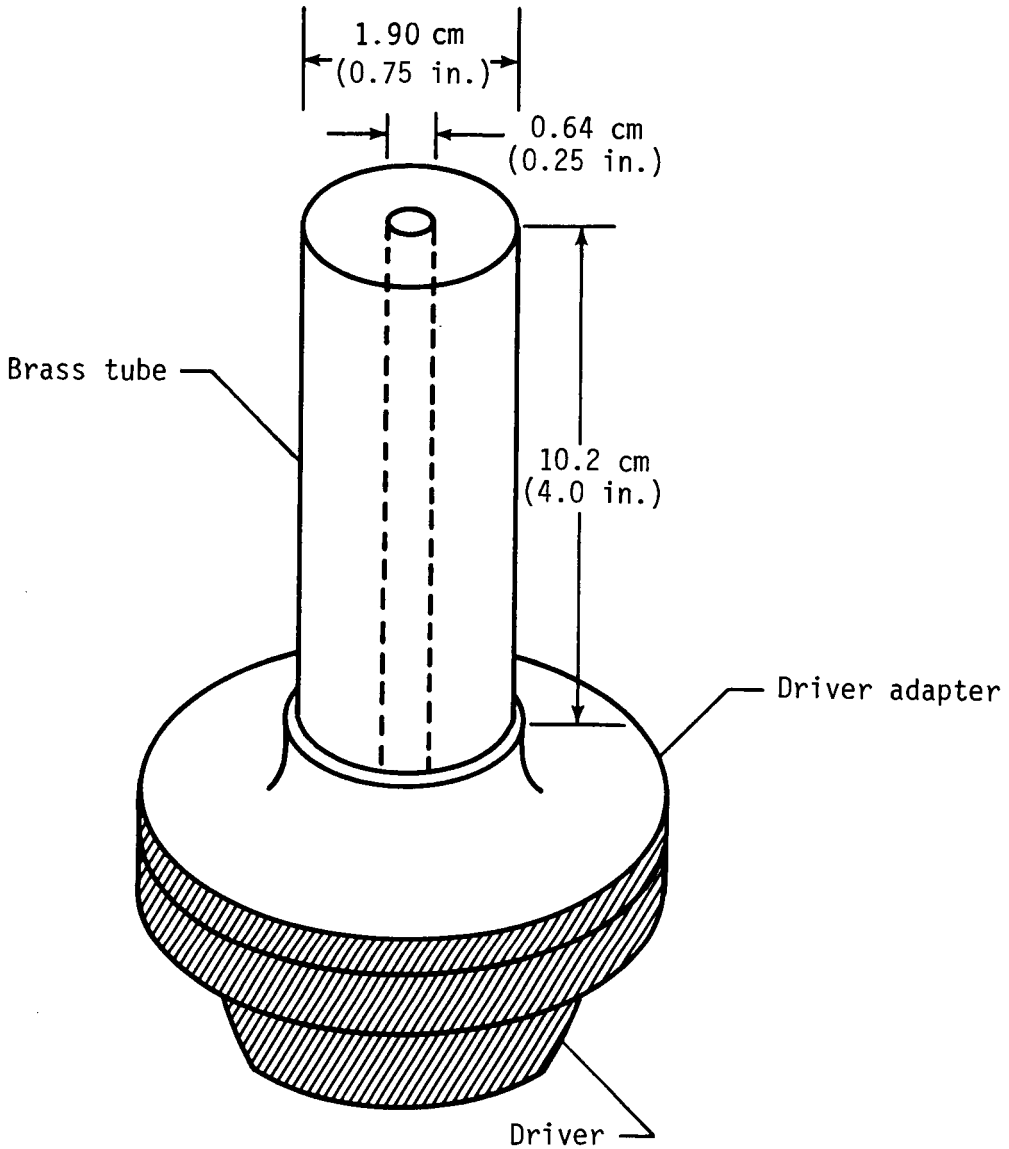

Figure 3. Sketch showing design of sound source.

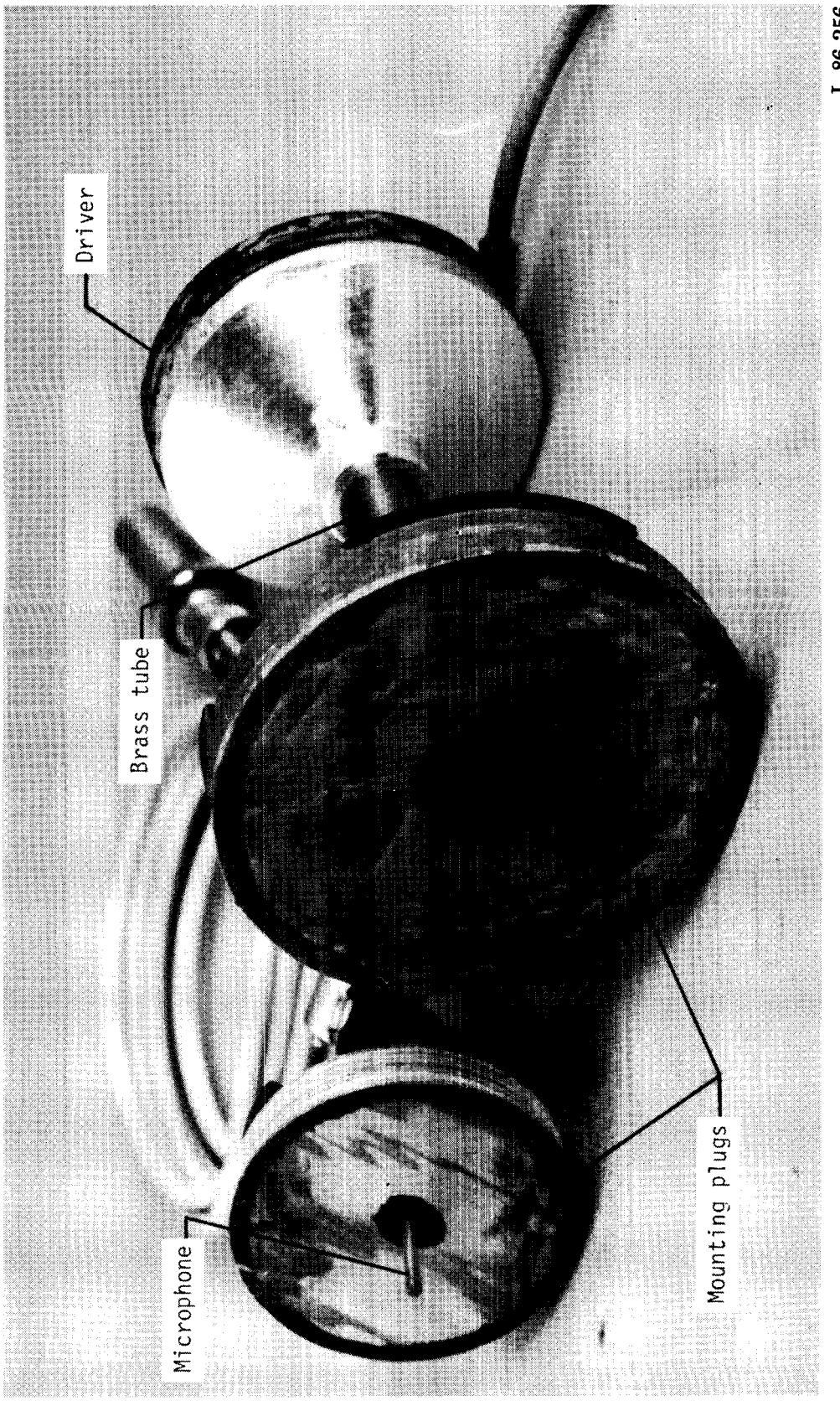

L-86-256

Figure 4. Photograph of front view of sound source and microphone assemblies.

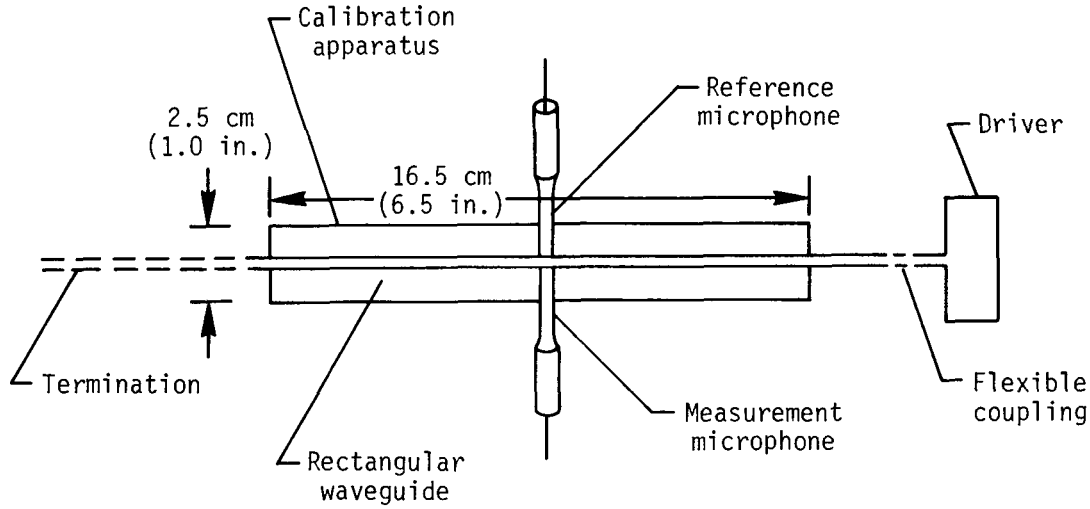

Figure 5. Schematic diagram of apparatus for calibrating microphone systems (relative frequency responses).

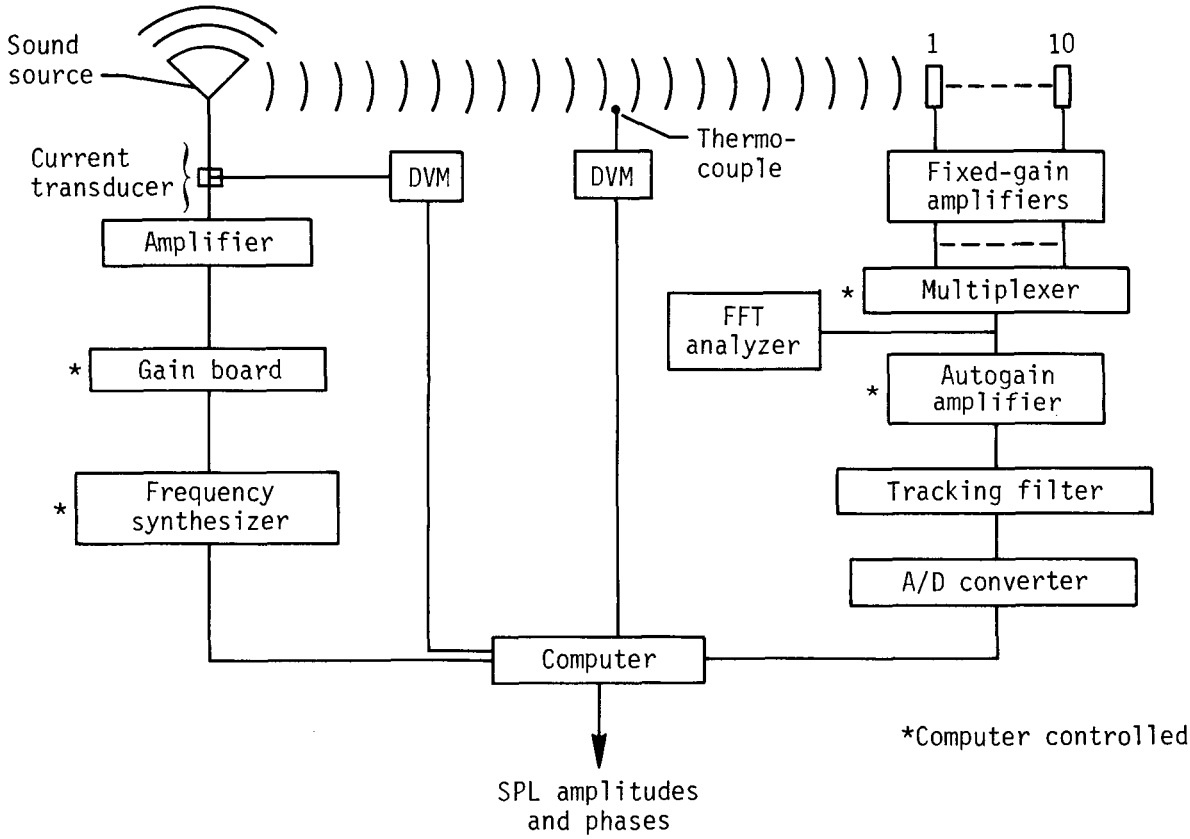

Figure 6. Schematic diagram of instrumentation layout.

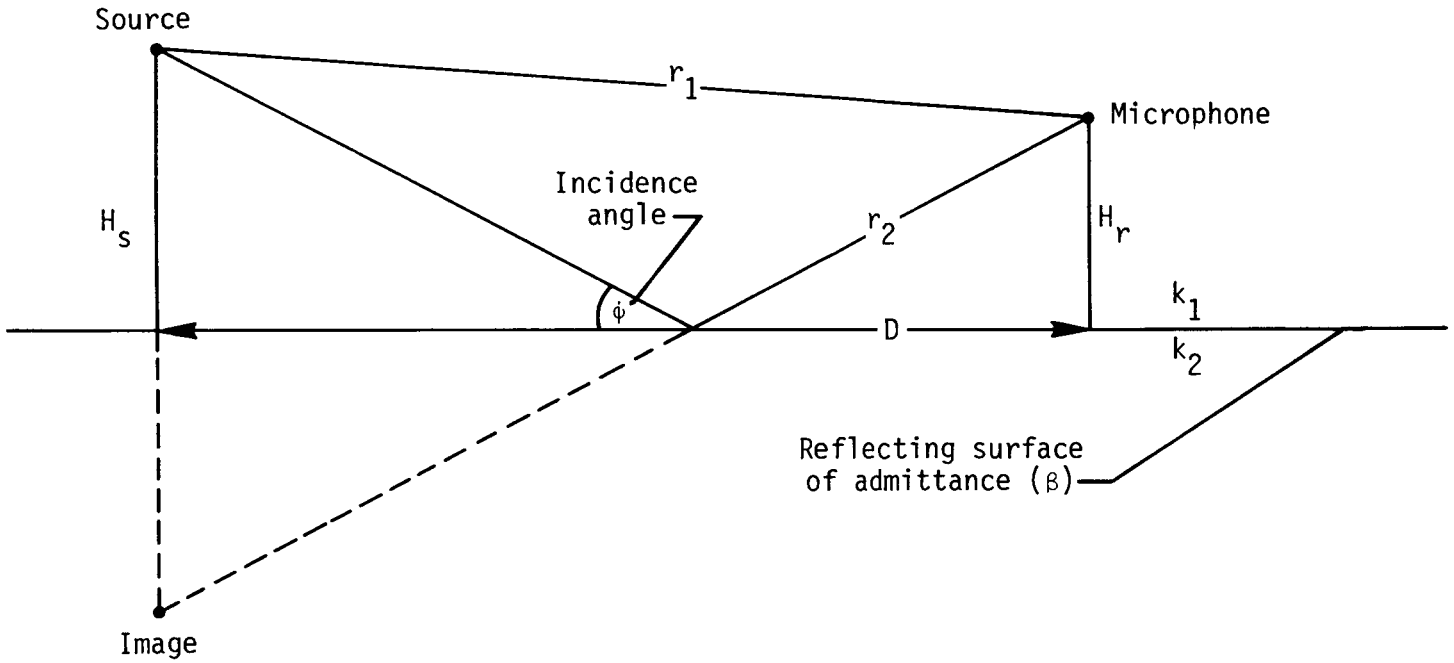

Figure 7. Sketch showing geometry of math model.

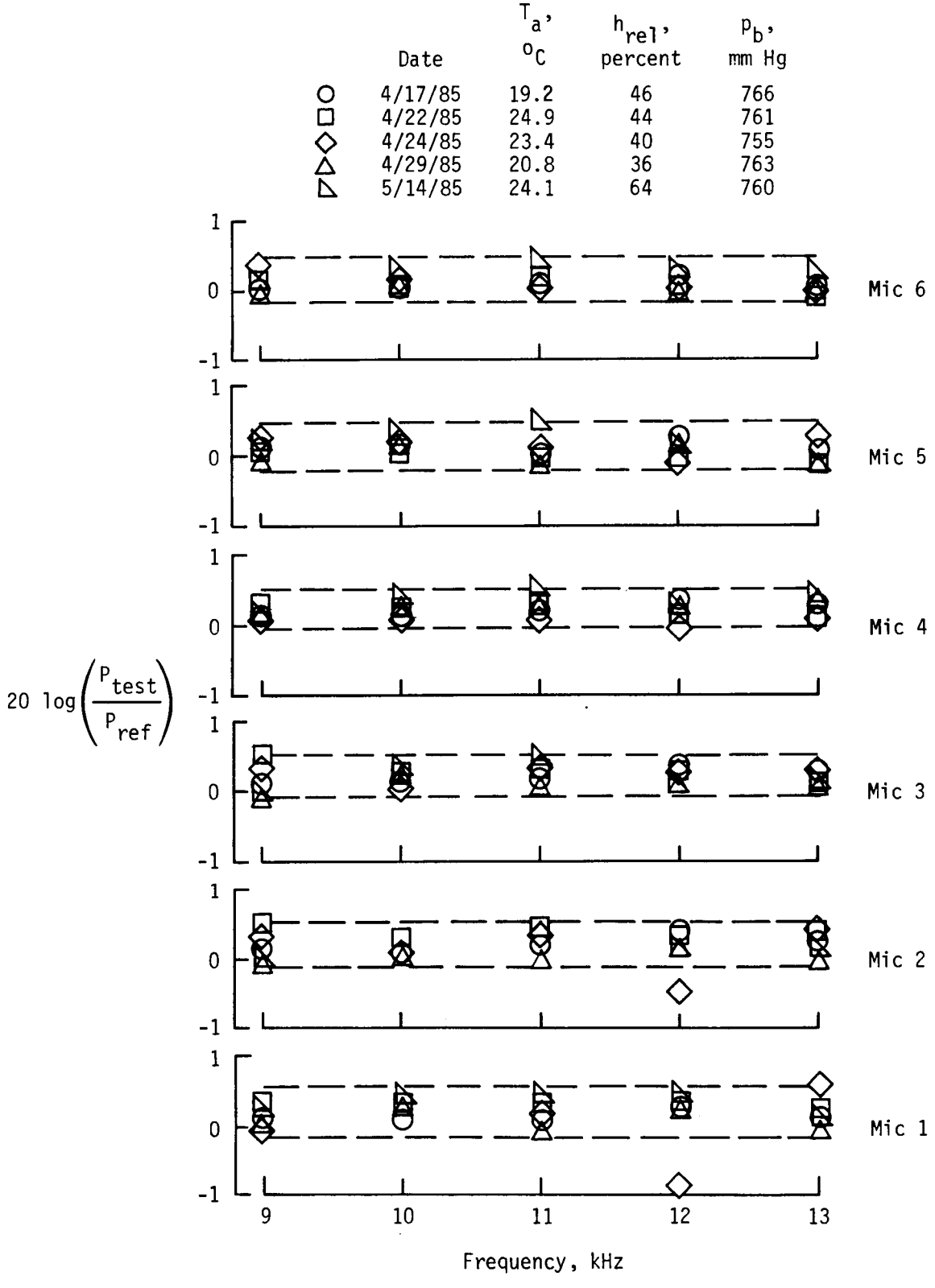

Figure 8. Frequency response comparisons for microphone systems.

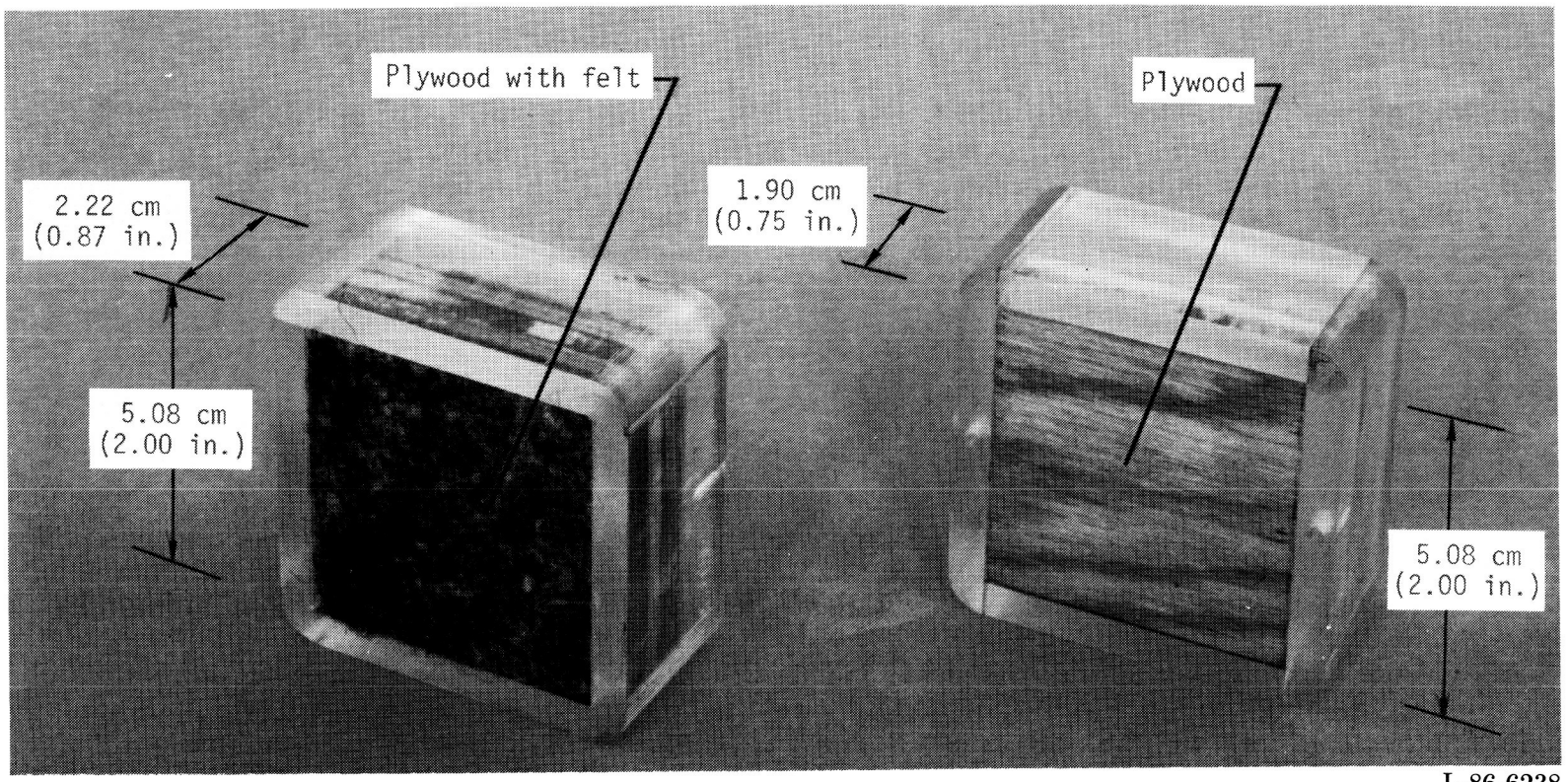

(a) Soft surface. (b) Hard surface.

Figure 9. Photograph of model-surface test specimens for impedance measurements.

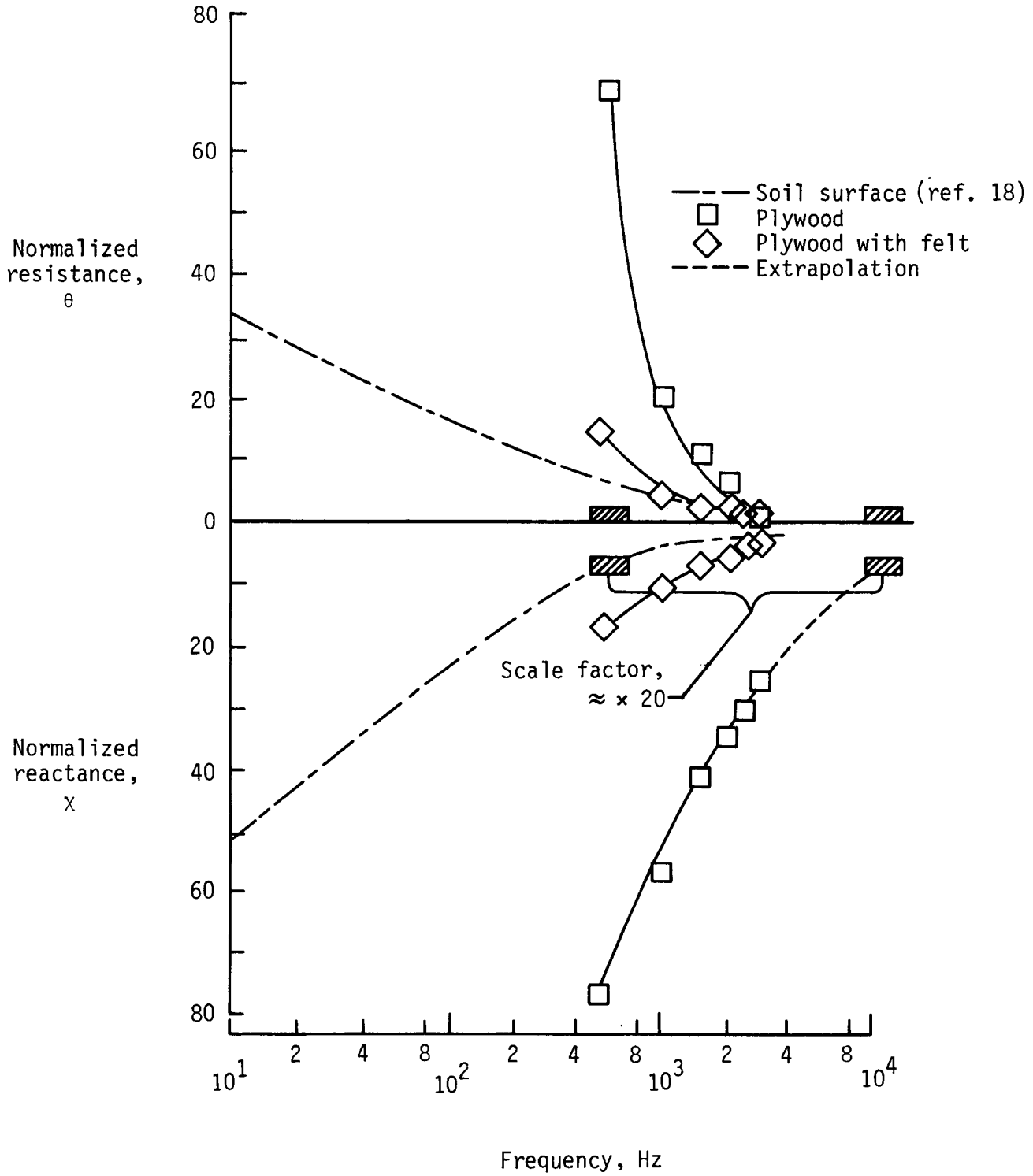

Figure 10. Comparison of normal-incidence impedances of model surfaces with that of soil surface.

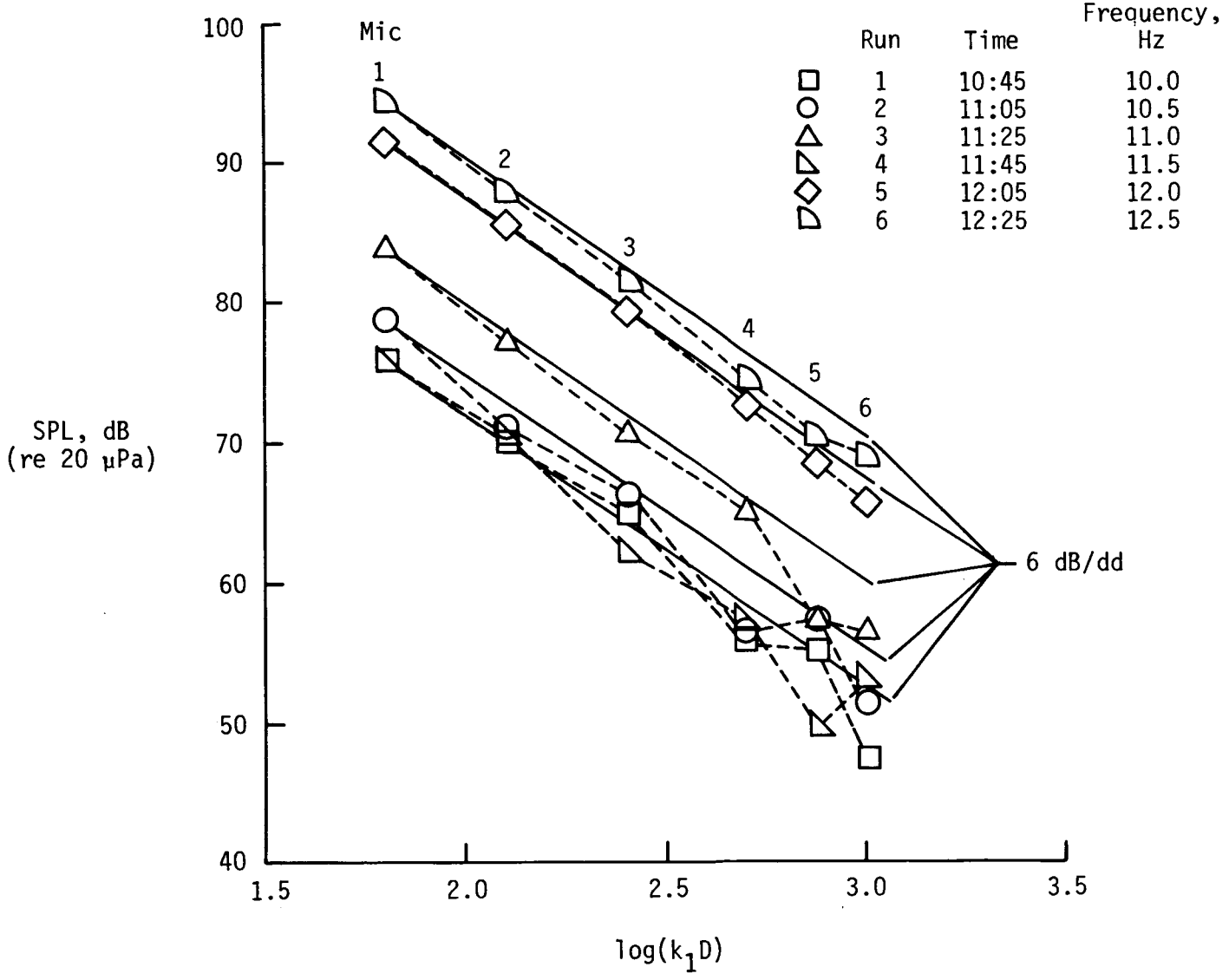

(a) Radial SPL distributions.

Figure 11. SPL distributions along radial and circular-arc arrays April 18, 1985, with outdoor windspeed of 1 knot, inside temperature of 19°C, and relative humidity of 40 percent. Hard surface; source and microphones at zero elevation.

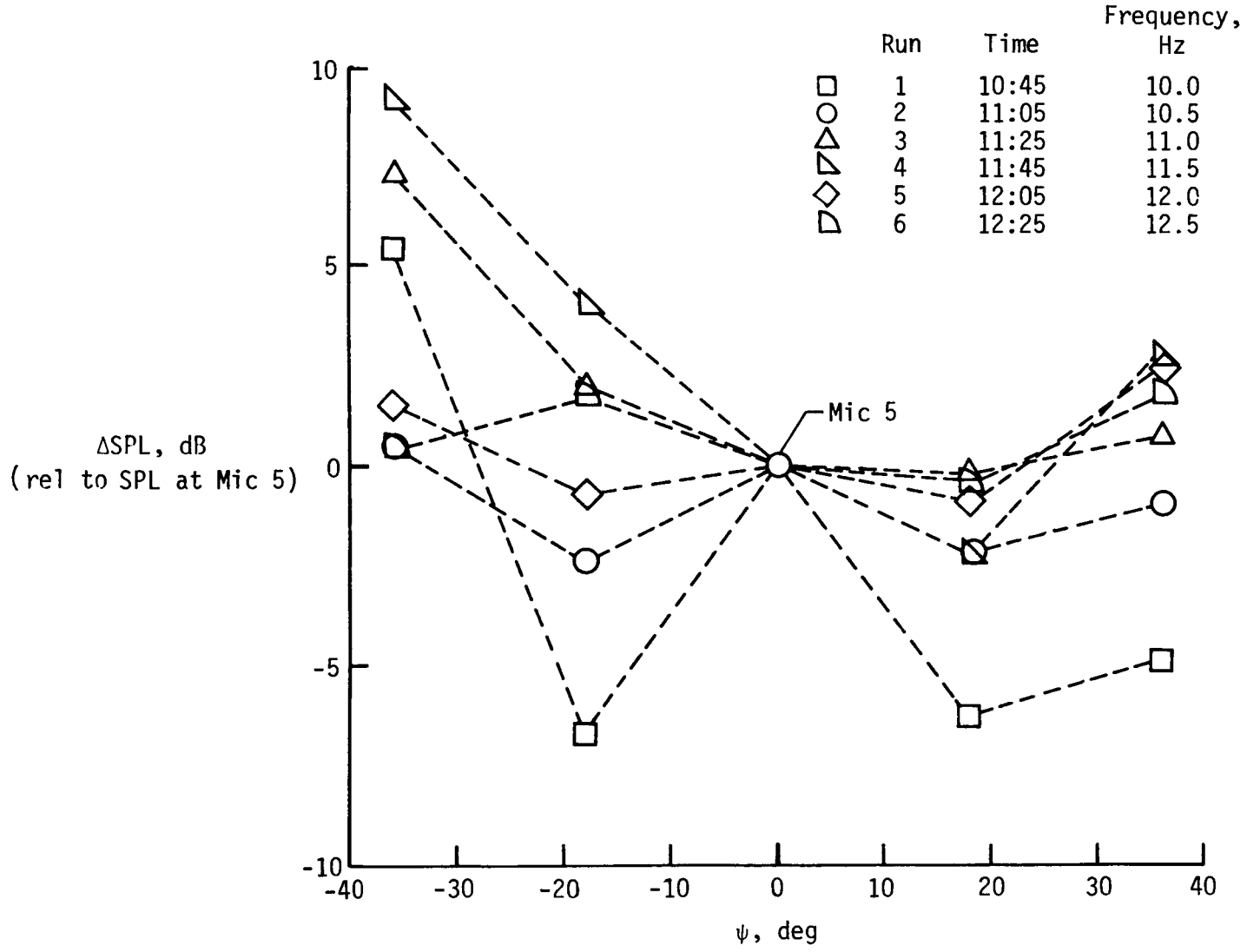

(b) Circular-arc SPL distributions.

Figure 11. Concluded.

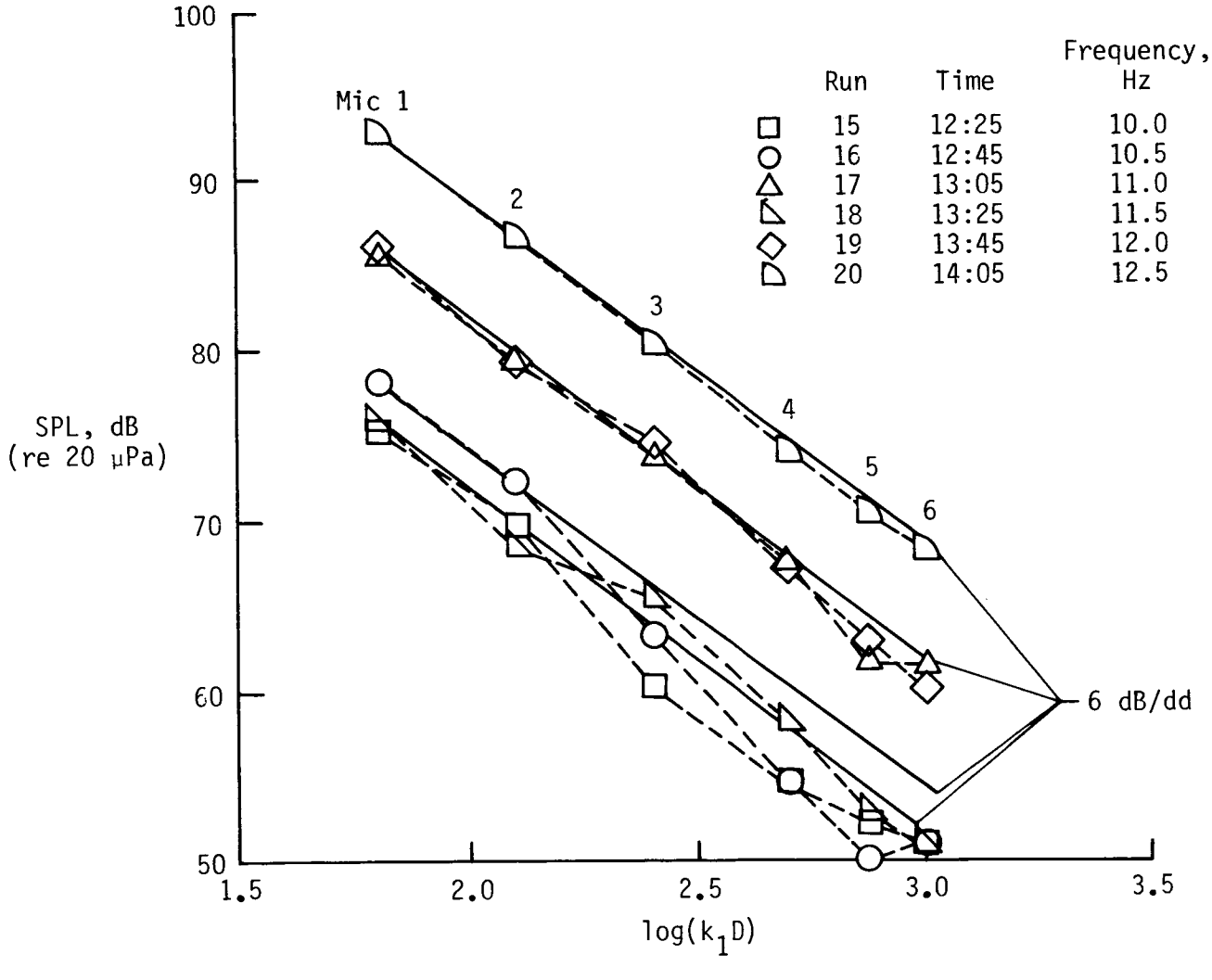

(a) Radial SPL distributions.

Figure 12. SPL distributions along radial and circular-arc arrays on April 22, 1985, with outdoor windspeed of 6 knots, inside temperature of 25°C, and relative humidity of 44 percent. Hard surface; source and microphones at zero elevation.

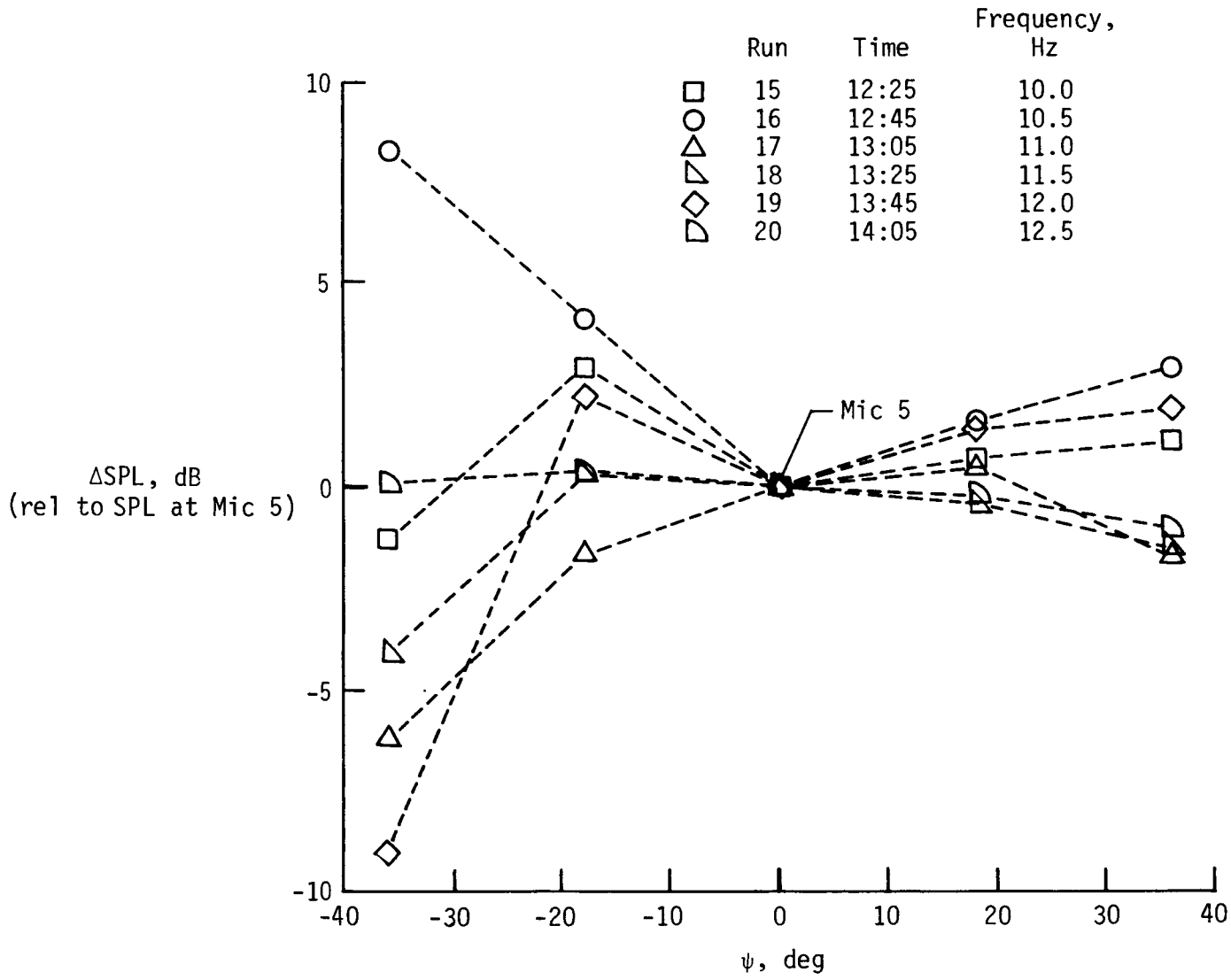

(b) Circular-arc SPL distributions.

Figure 12. Concluded.

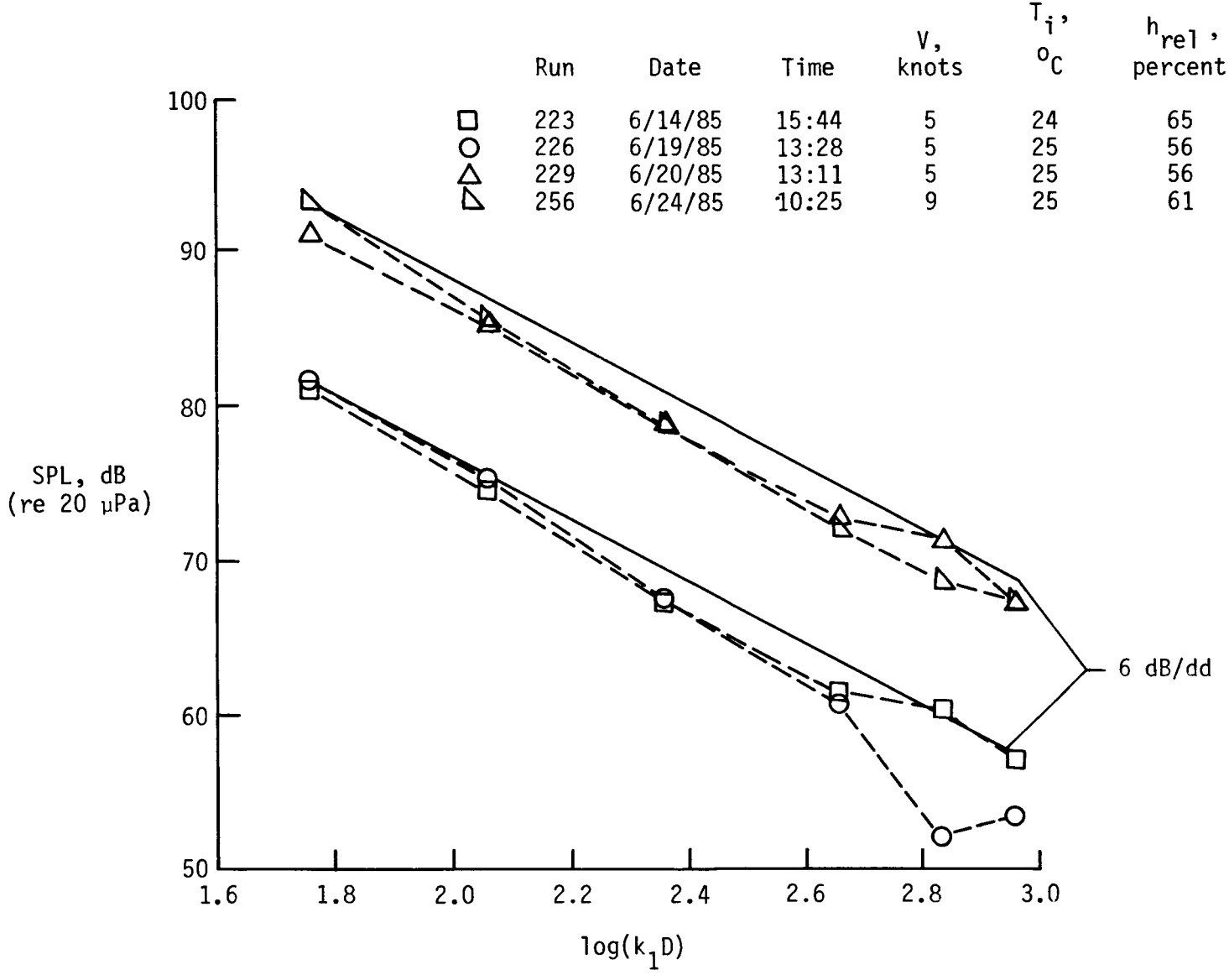

Figure 13. SPL distributions along radial array at frequency of 9.0 kHz for hard surface with source and microphone at zero elevation.

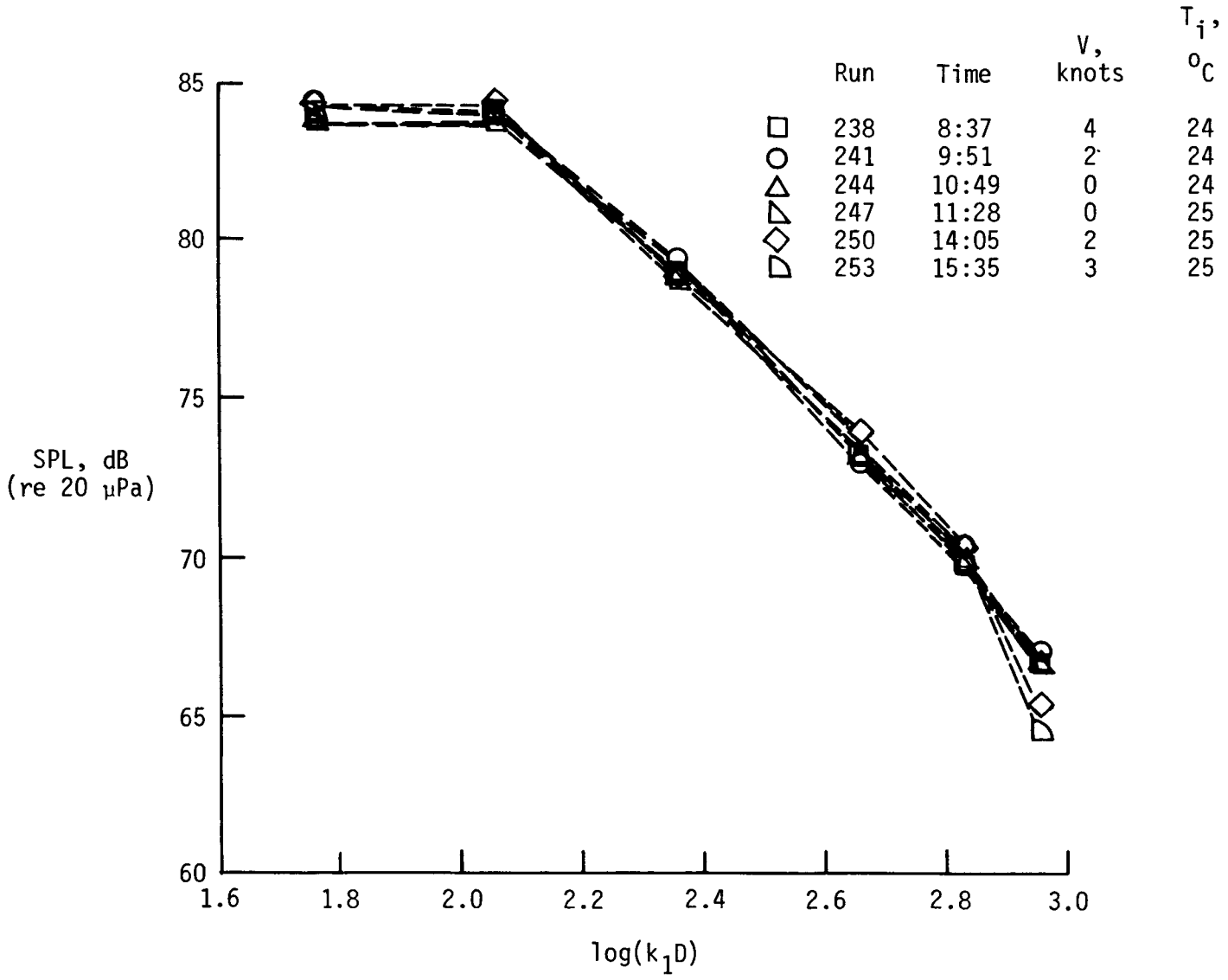

Figure 14. SPL distributions along radial array on June 21, 1985, at frequency of 9.0 kHz and relative humidity of 54 percent. Hard surface; source and microphones at elevations of 5.84 and 3.56 cm.

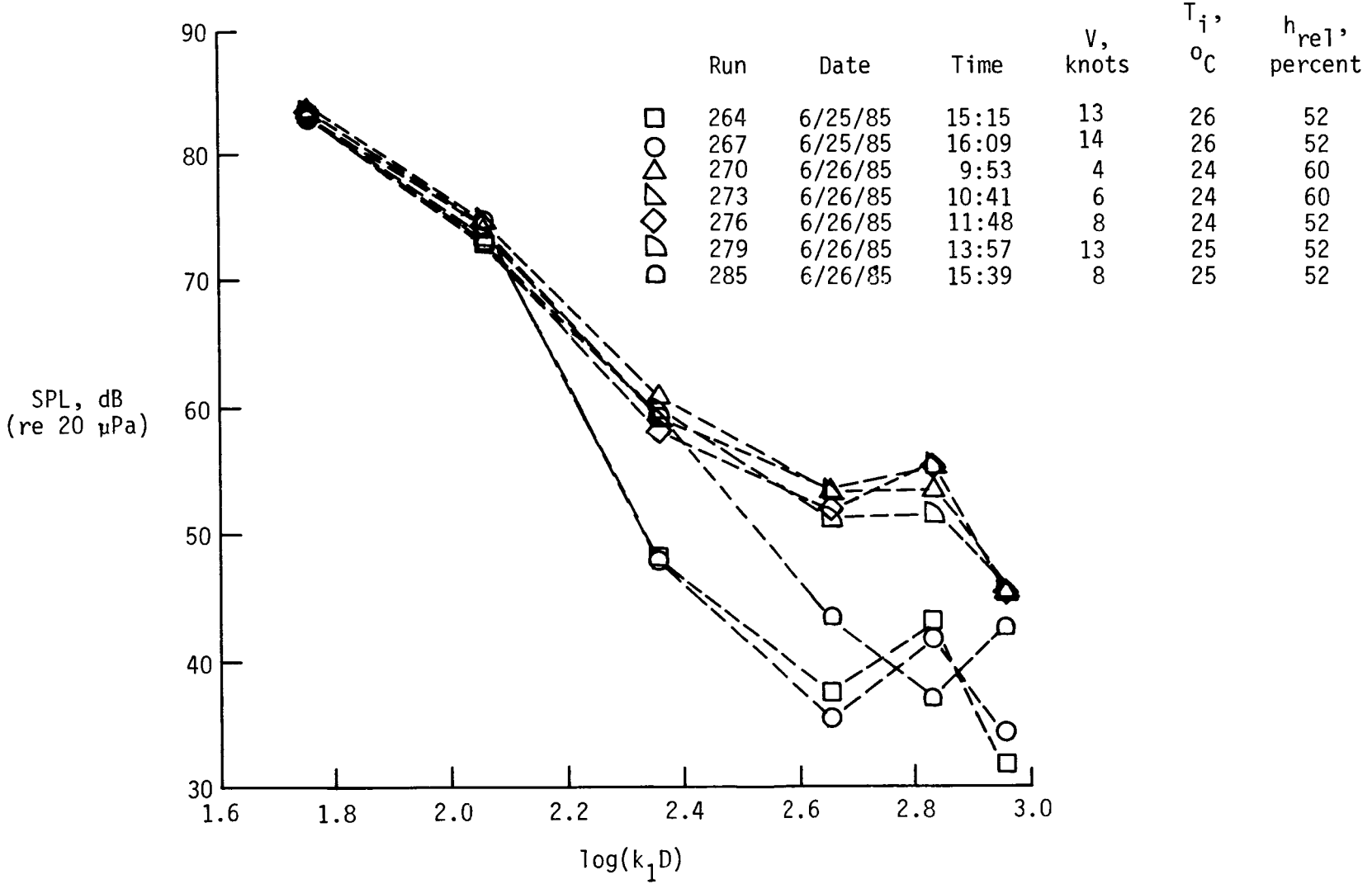

Figure 15. SPL distributions along radial array at frequency of 9.0 kHz for soft surface with source and microphones at elevations of 5.84 and 3.56 cm.

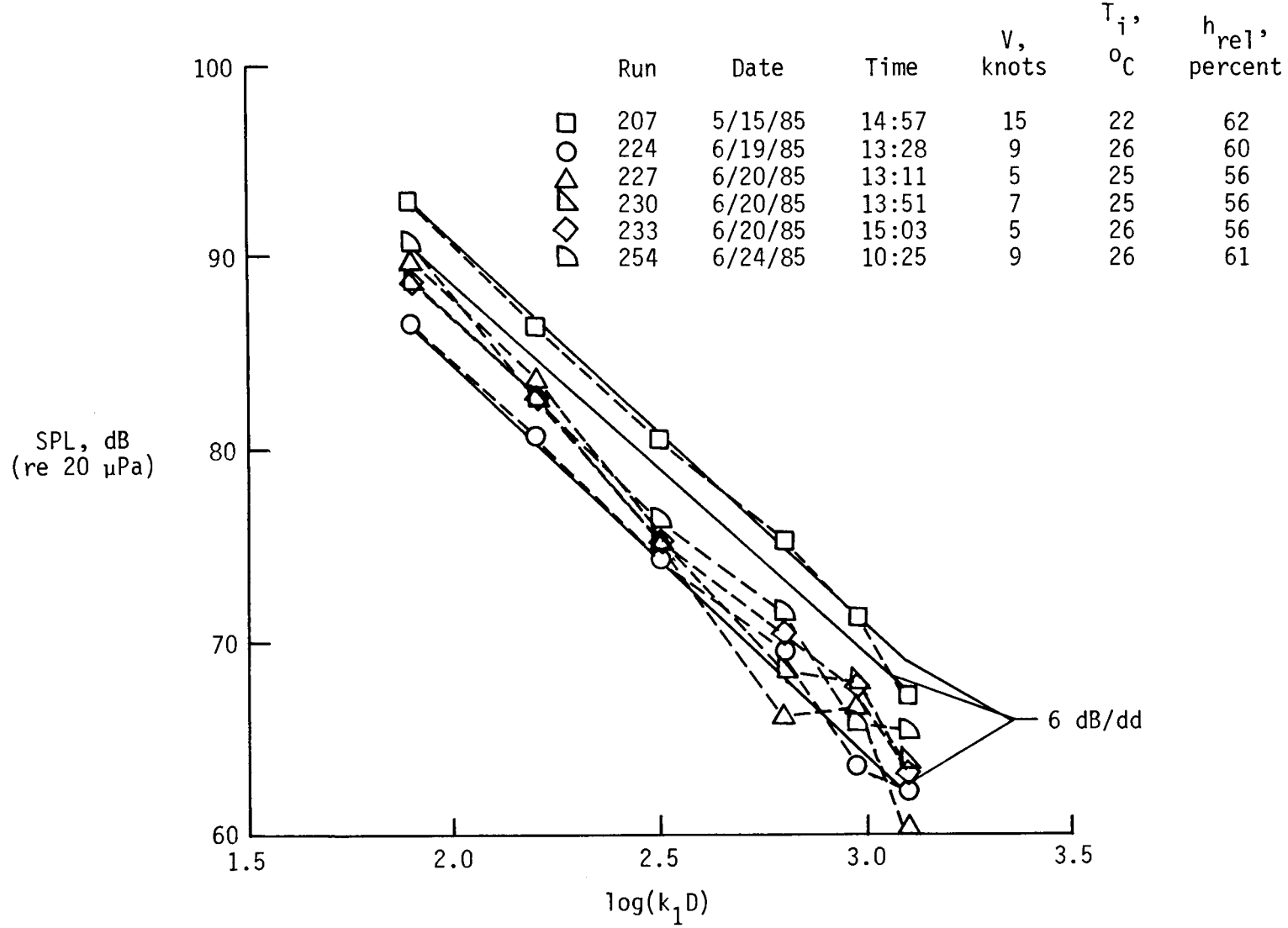

Figure 16. SPL distributions along radial array at frequency of 12.5 kHz for hard surface with source and microphones at zero elevation.

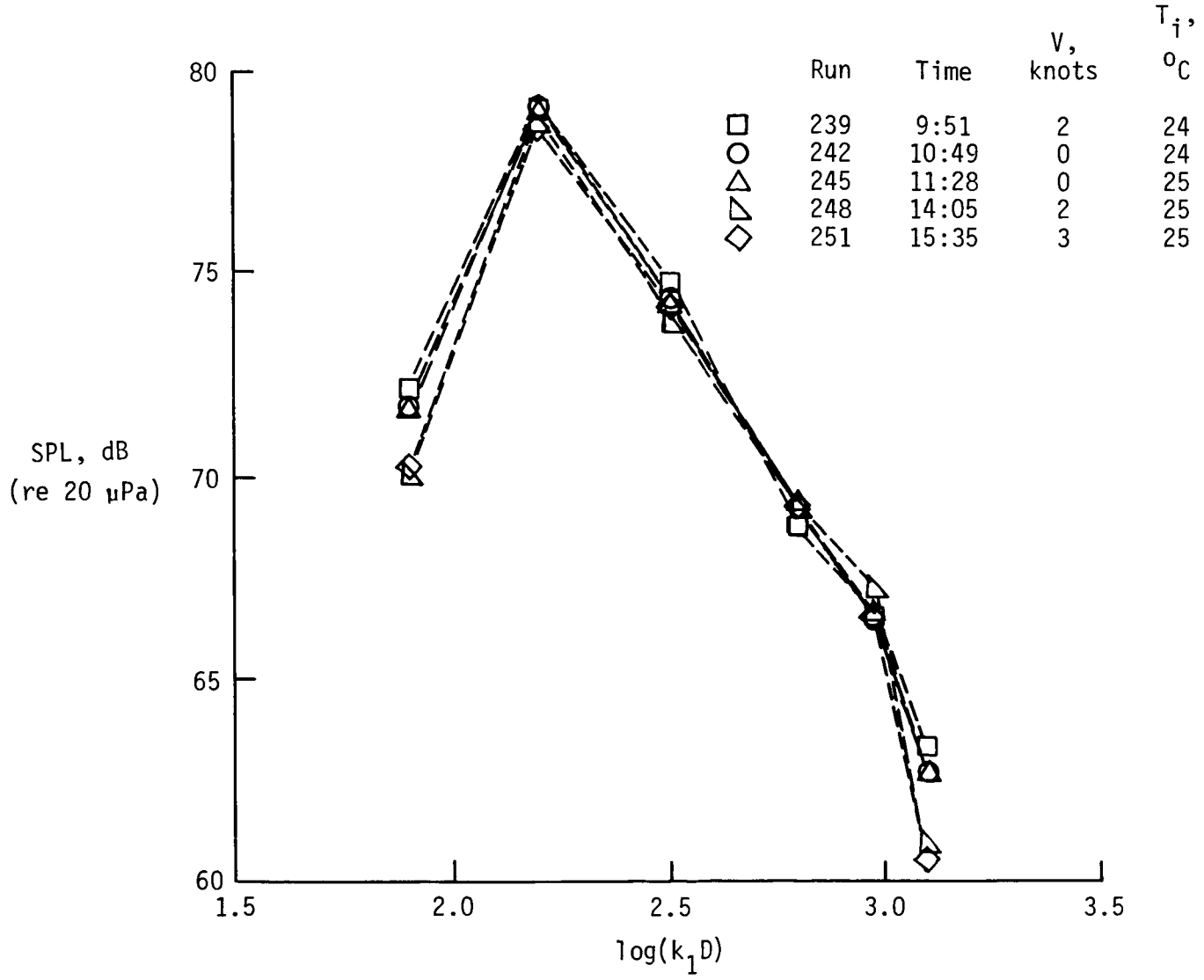

Figure 17. SPL distributions along radial array on June 21, 1985, at frequency of 12.5 kHz and relative humidity of 54 percent. Hard surface; source and microphones at elevations of 5.84 and 3.56 cm.

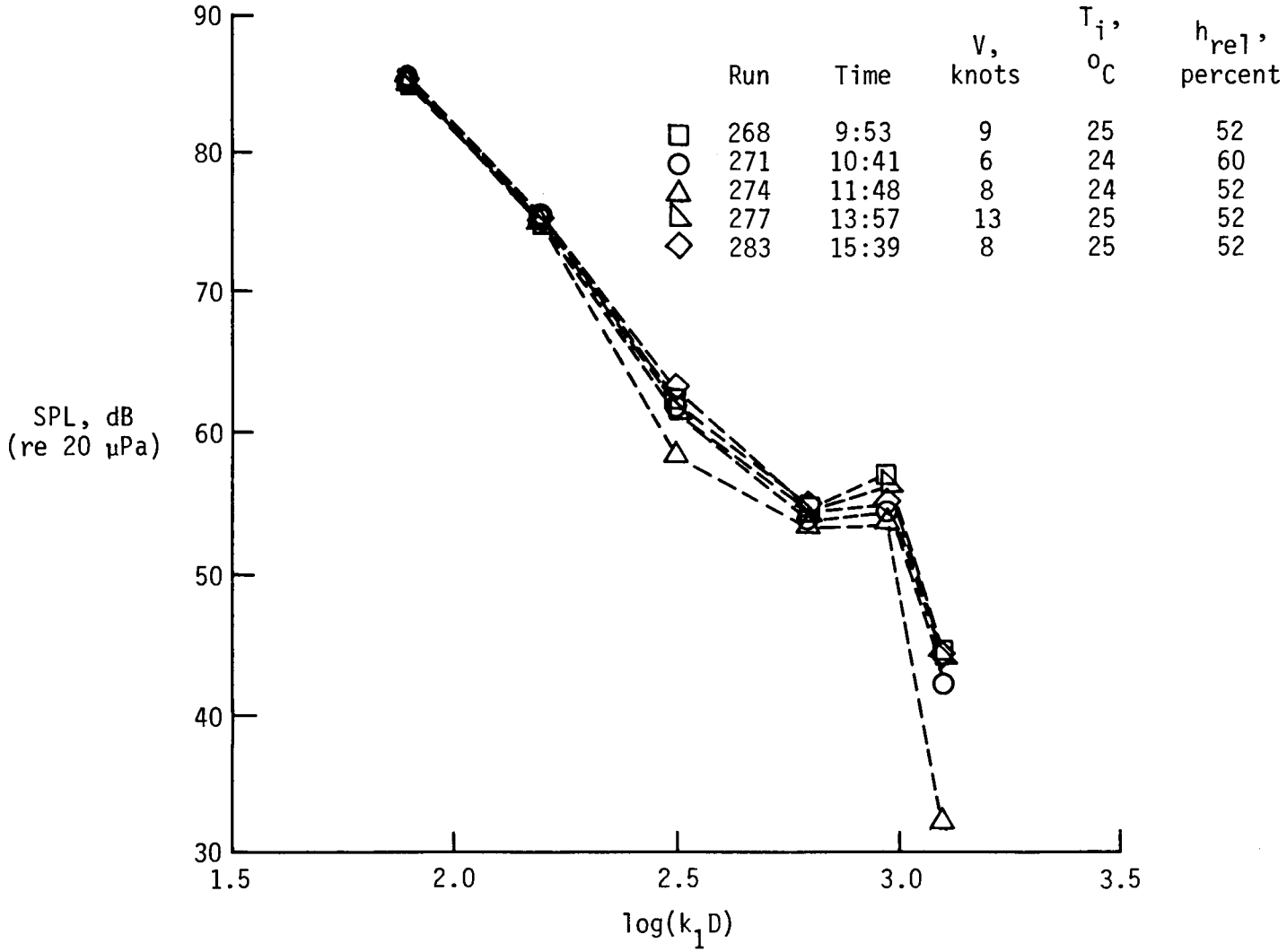

Figure 18. SPL distributions along radial array on June 26, 1985, at frequency of 12.5 kHz. Soft surface; source and microphones at elevations of 5.84 and 3.56 cm.

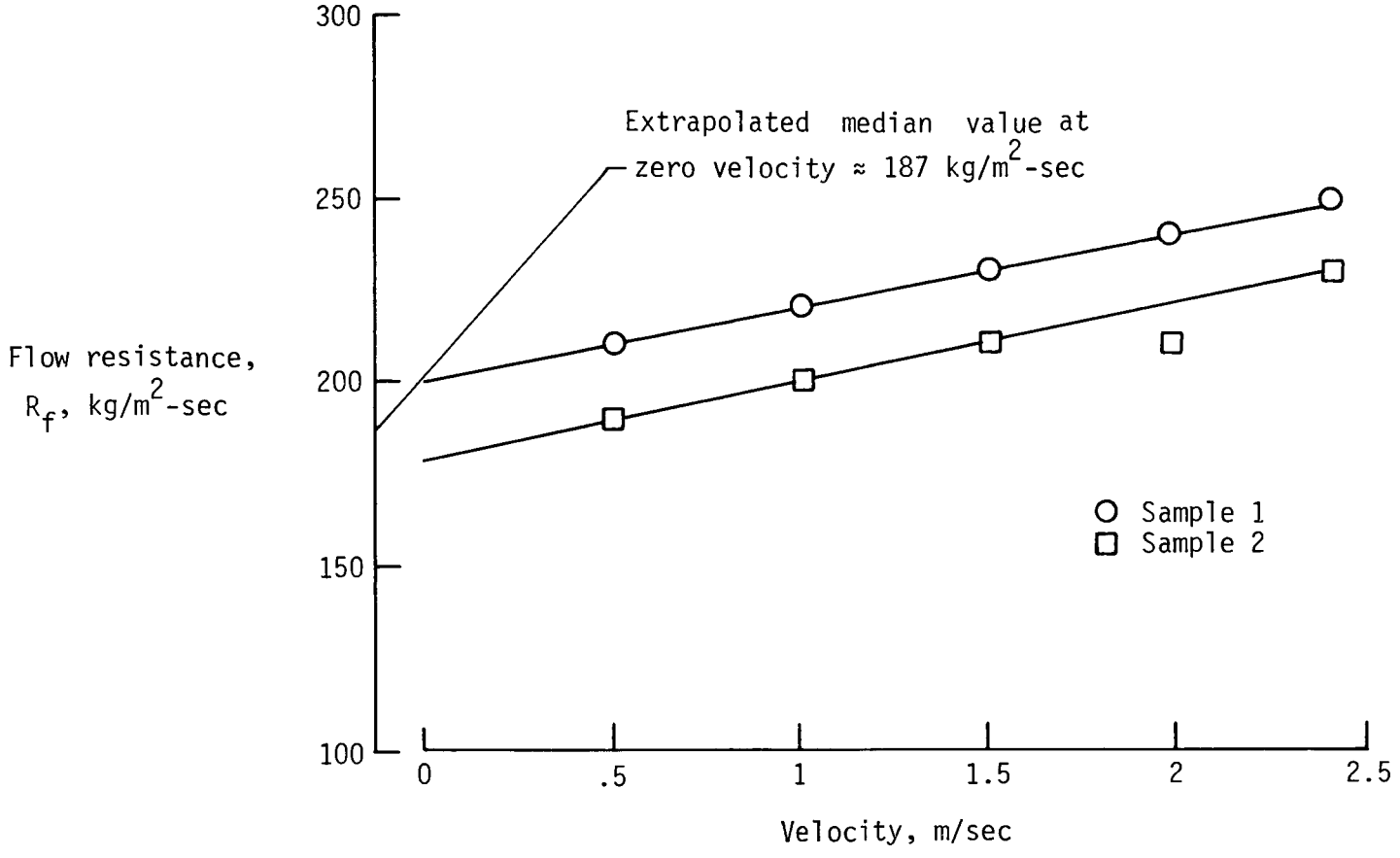

Figure 19. Measured flow resistance of felt covering. $R_1 \approx 5.9 \times 10^4$ kg/m^3-sec.

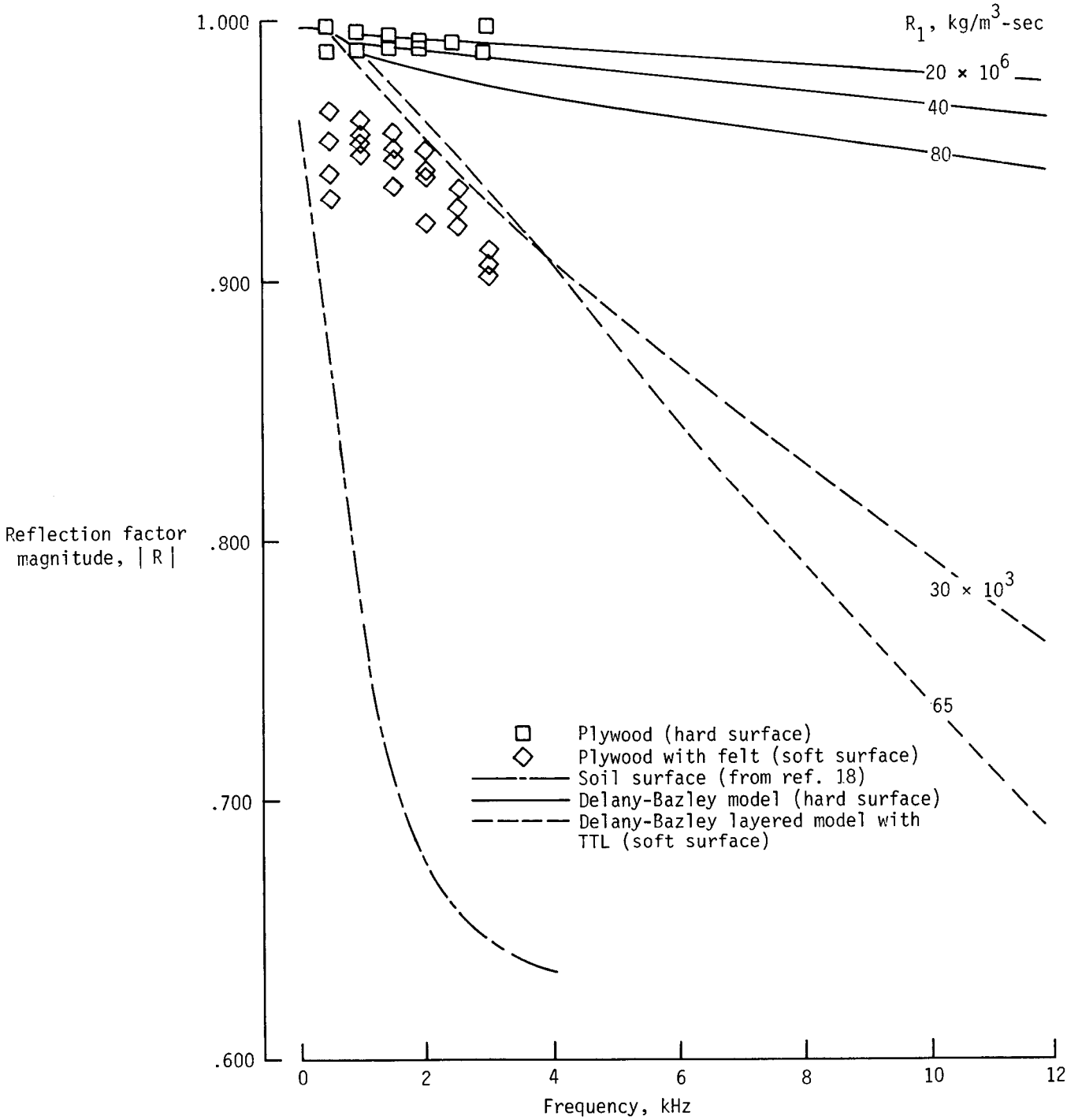

Figure 20. Comparison of measured and calculated reflection factor magnitudes for hard and soft model surfaces.

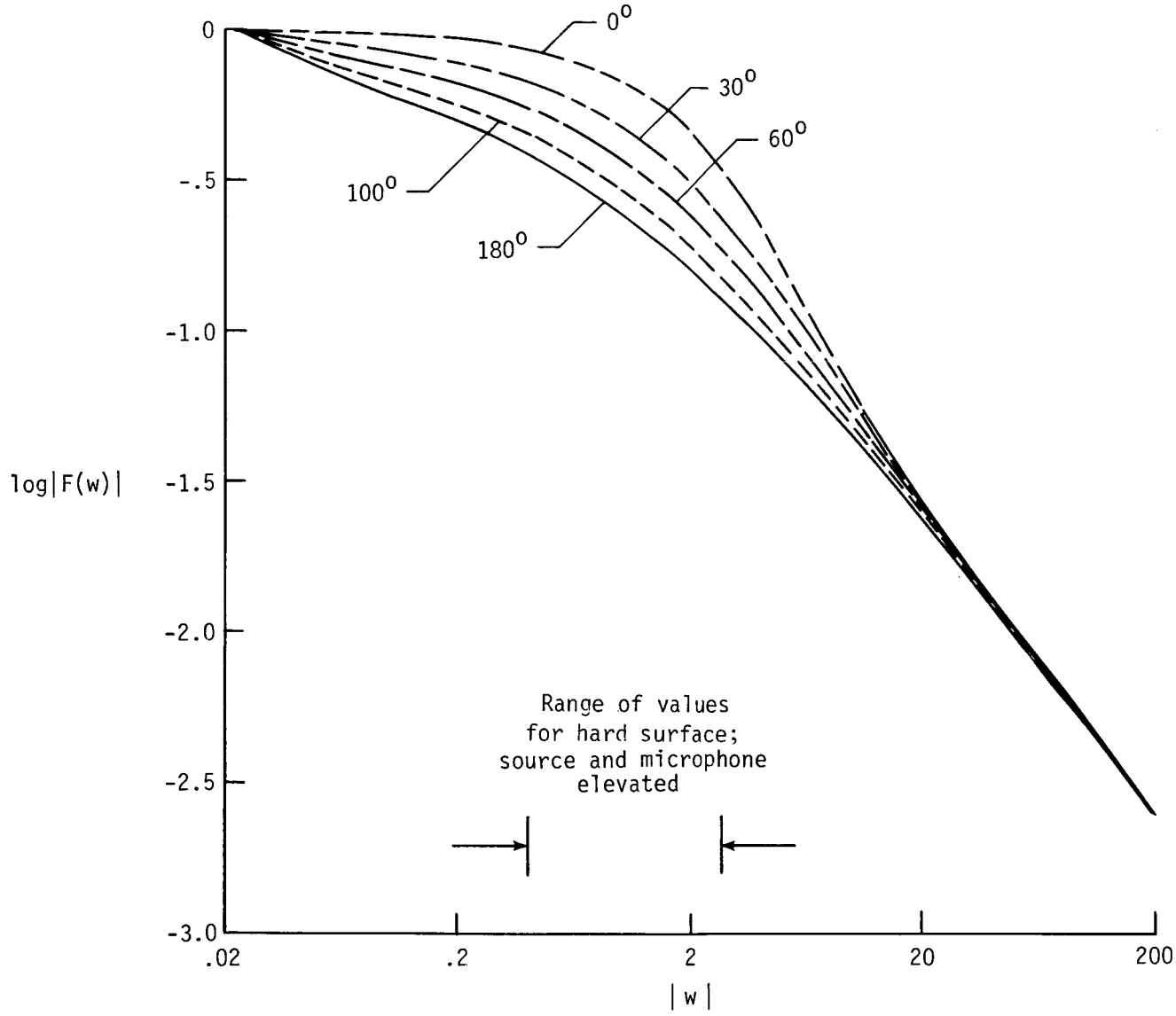

(a) Phase range of w from 0° to 180°.

Figure 21. Log of boundary-loss factor versus magnitude of numerical distance.

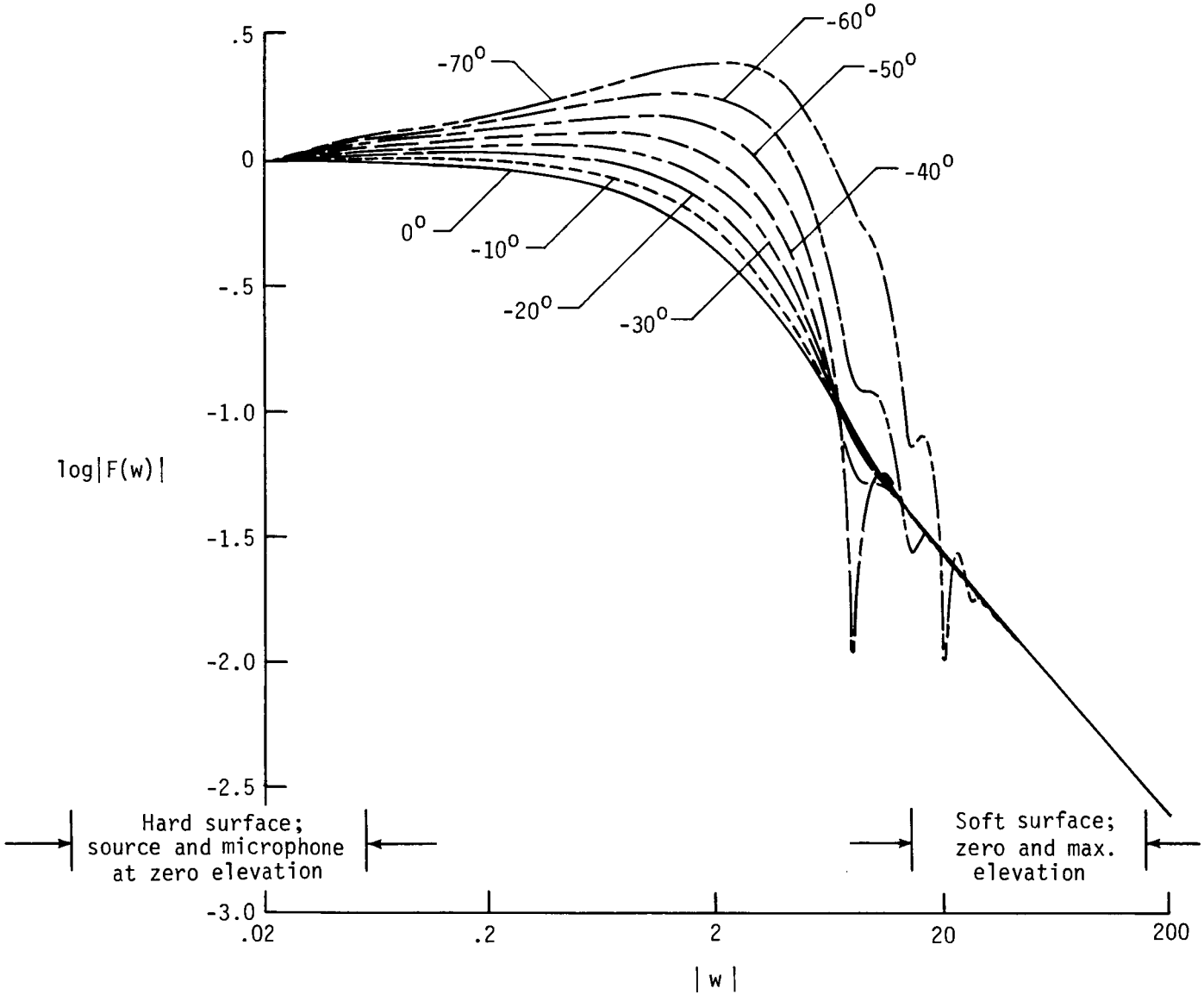

(b) Phase range of w from 0° to −70°.

Figure 21. Concluded.

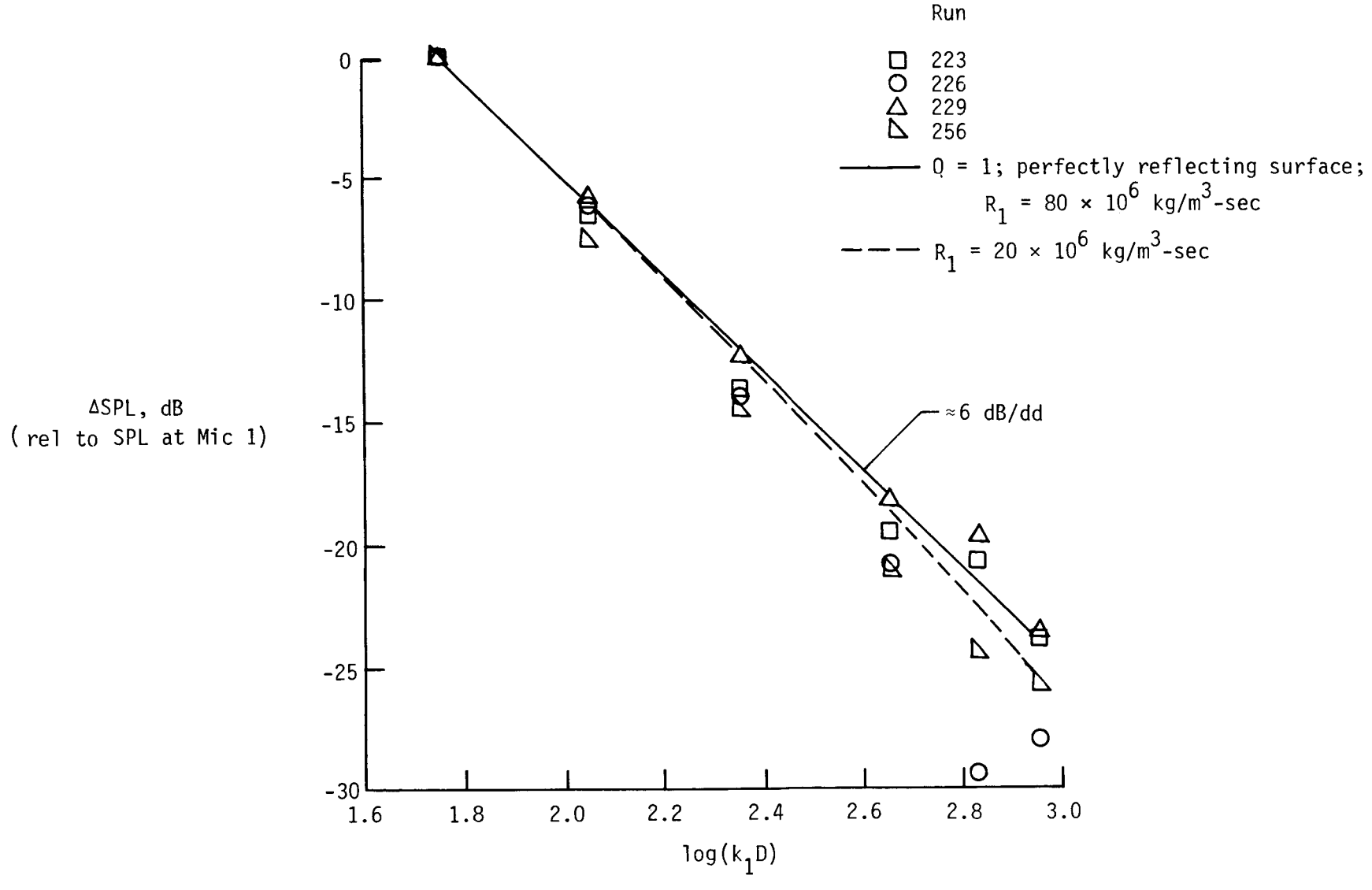

Figure 22. Comparison of measured and calculated changes in radial SPL distributions at frequency of 9.0 kHz for hard surface with source and microphones at zero elevation.

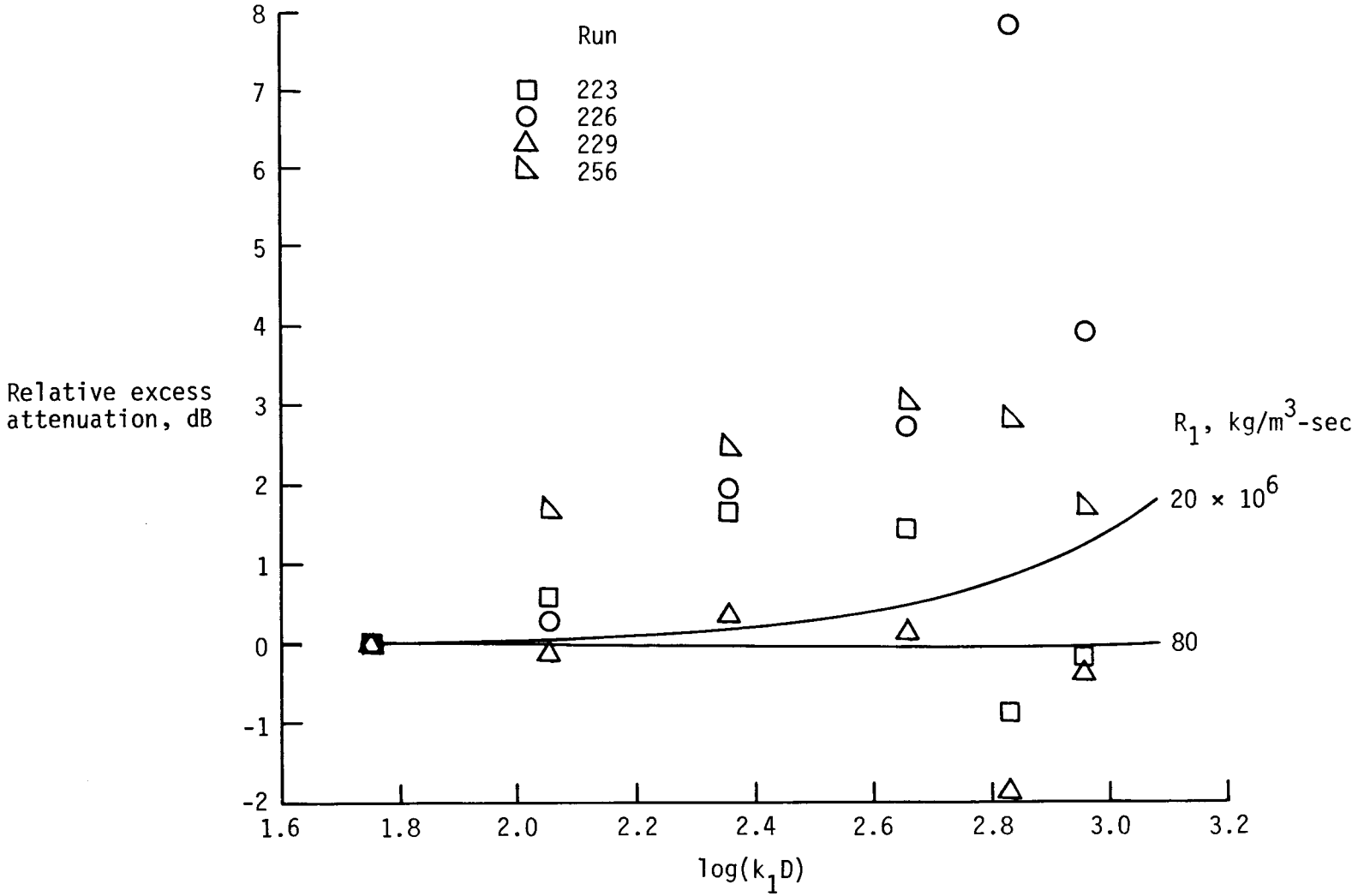

Figure 23. Comparison of measured and calculated relative excess attenuation for two values of R_1 at frequency of 9.0 kHz and outside temperature of 25°C. Hard surface; source and microphones at zero elevation.

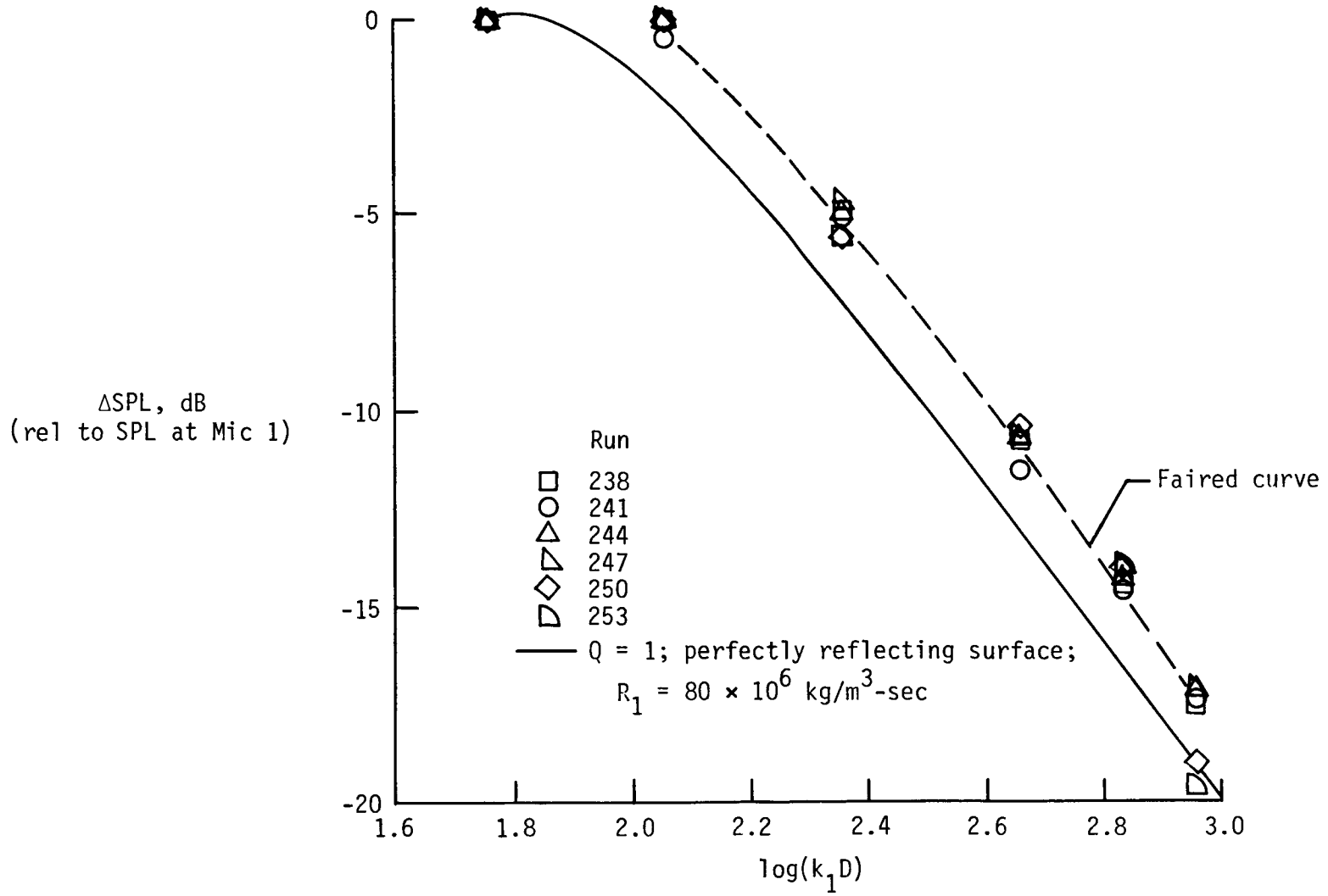

Figure 24. Comparison of measured and calculated changes in radial SPL distributions at frequency of 9.0 kHz for hard surface with source and microphones at elevations of 5.84 and 3.56 cm.

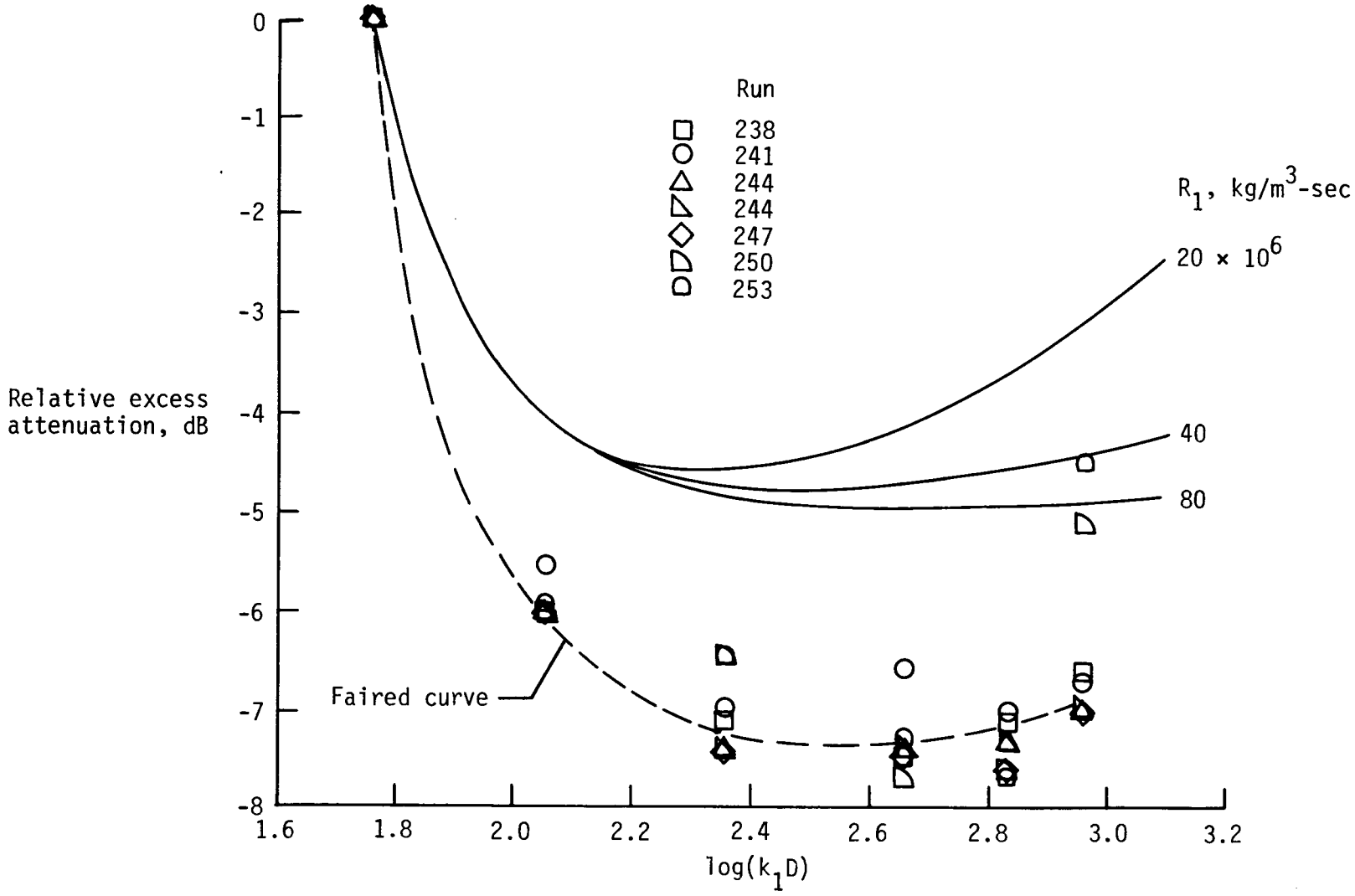

Figure 25. Comparison of measured and calculated relative excess attenuation for three values of R_1 at frequency of 9.0 kHz and inside temperature of 25°C. Hard surface; source and microphones at elevations of 5.84 and 3.56 cm.

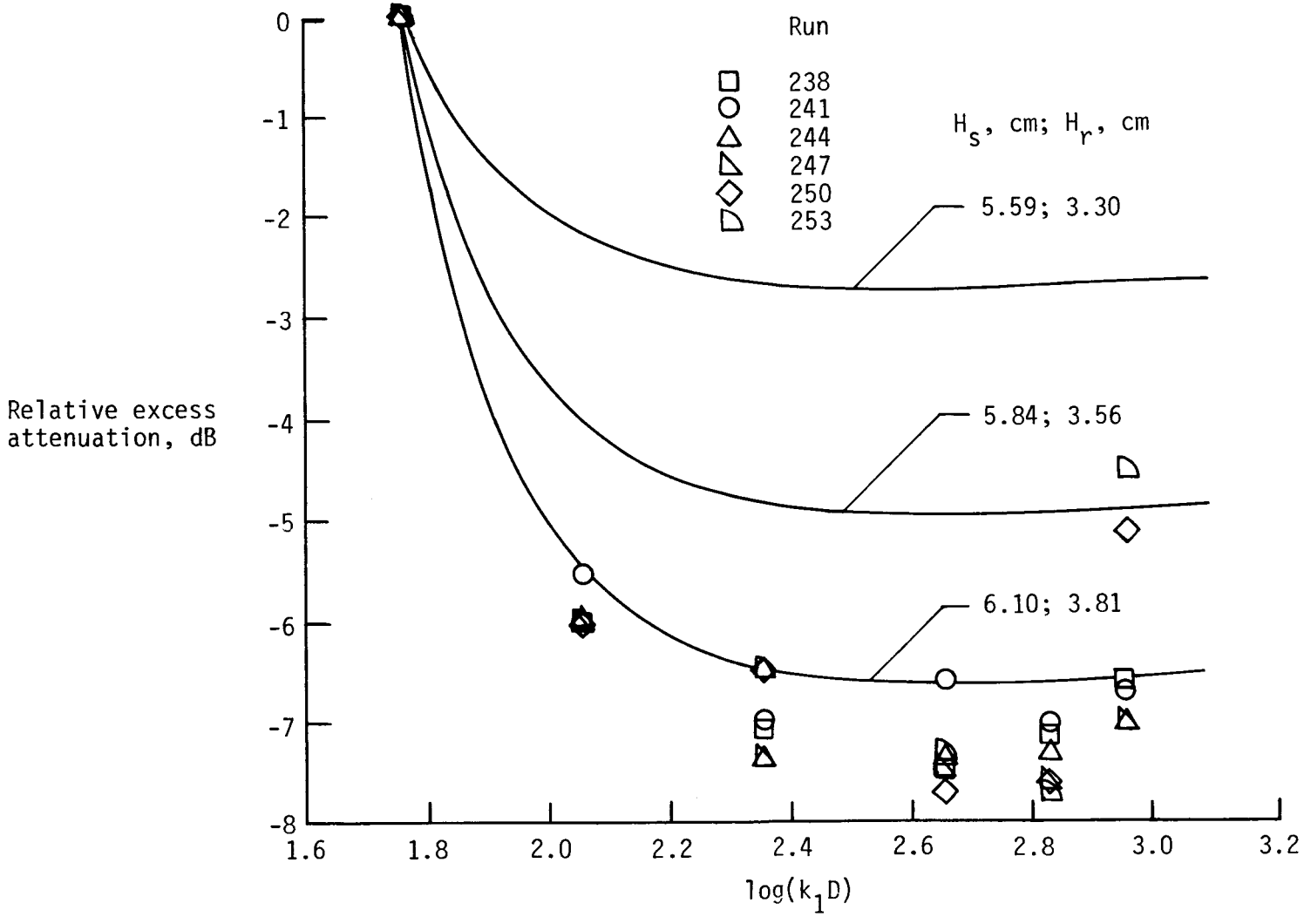

Figure 26. Comparison of measured and calculated relative excess attenuation for three source and microphone elevations at frequency of 9.0 kHz, inside temperature of 25°C, and $R_1 = 80 \times 10^6$ kg/m^3-sec for hard surface.

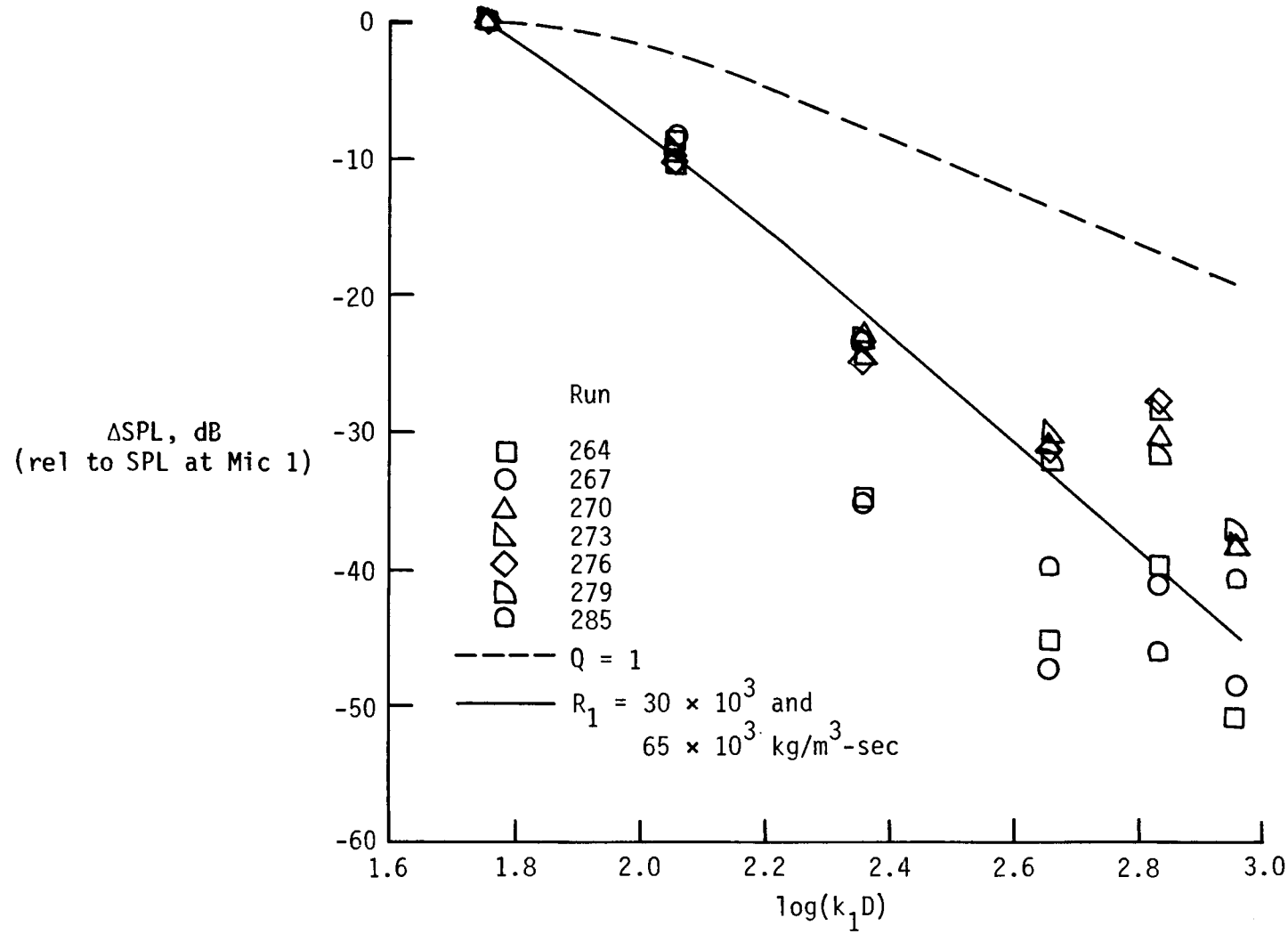

Figure 27. Comparison of measured and calculated changes in radial SPL distributions at frequency of 9.0 kHz and inside temperature of 26°C. Soft surface; source and microphones at elevations of 5.84 and 3.56 cm.

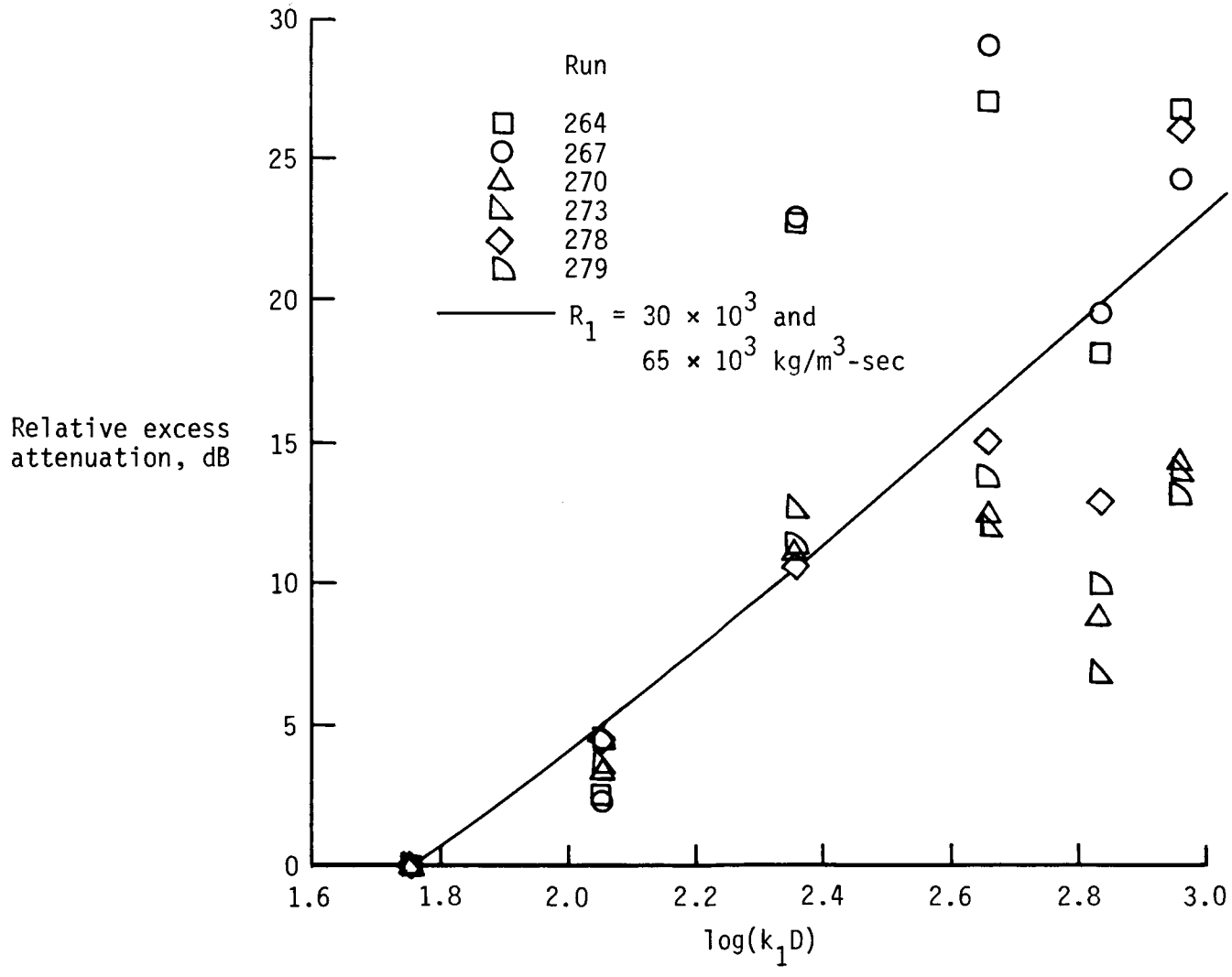

Figure 28. Comparison of measured and calculated relative excess attenuation at frequency of 9.0 kHz and inside temperature of 25°C. Soft surface; source and microphones at elevations of 5.84 and 3.56 cm.

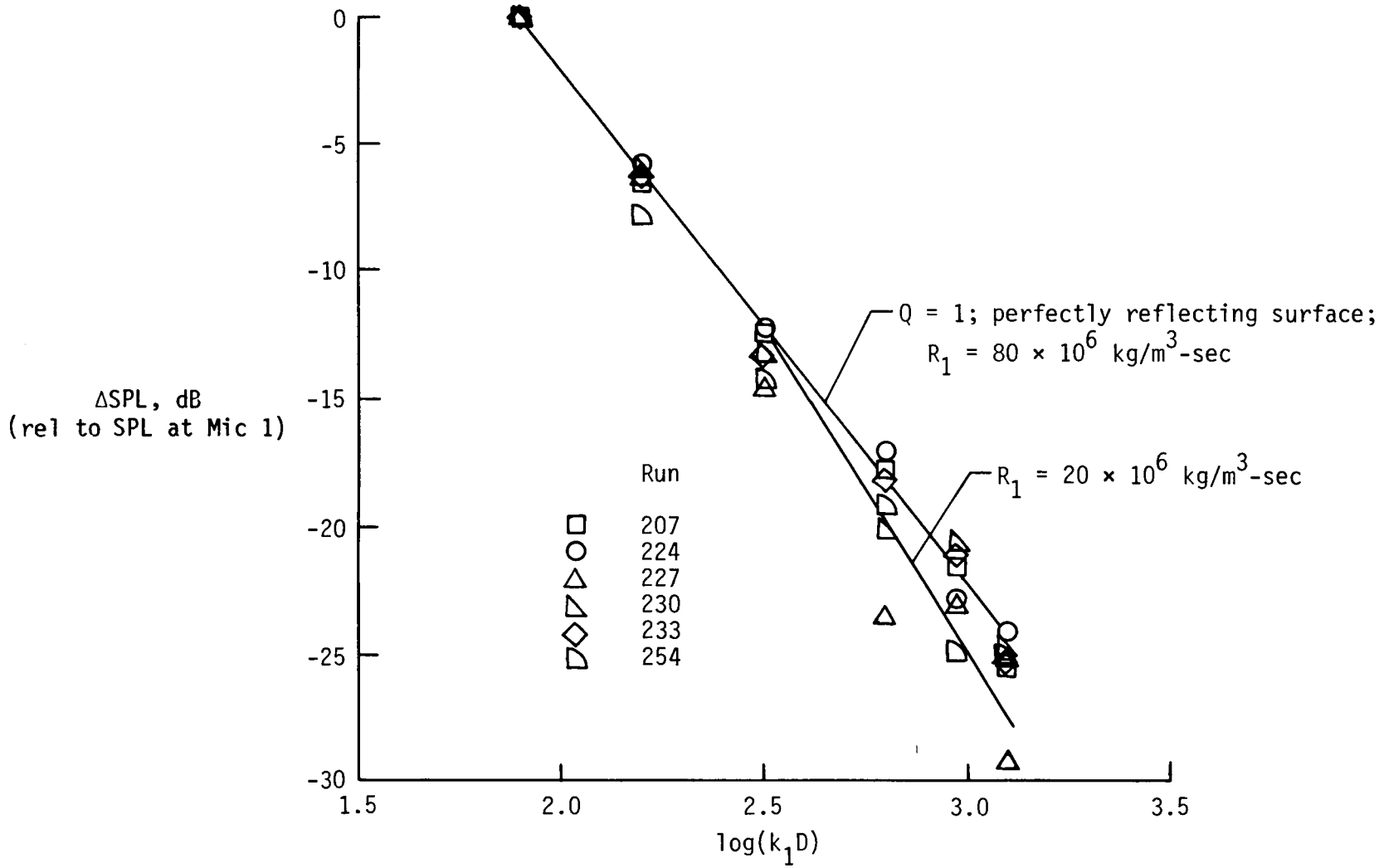

Figure 29. Comparison of measured and calculated changes in radial SPL distributions at frequency of 12.5 kHz and inside temperature of 25°. Hard surface; source and microphones at zero elevation.

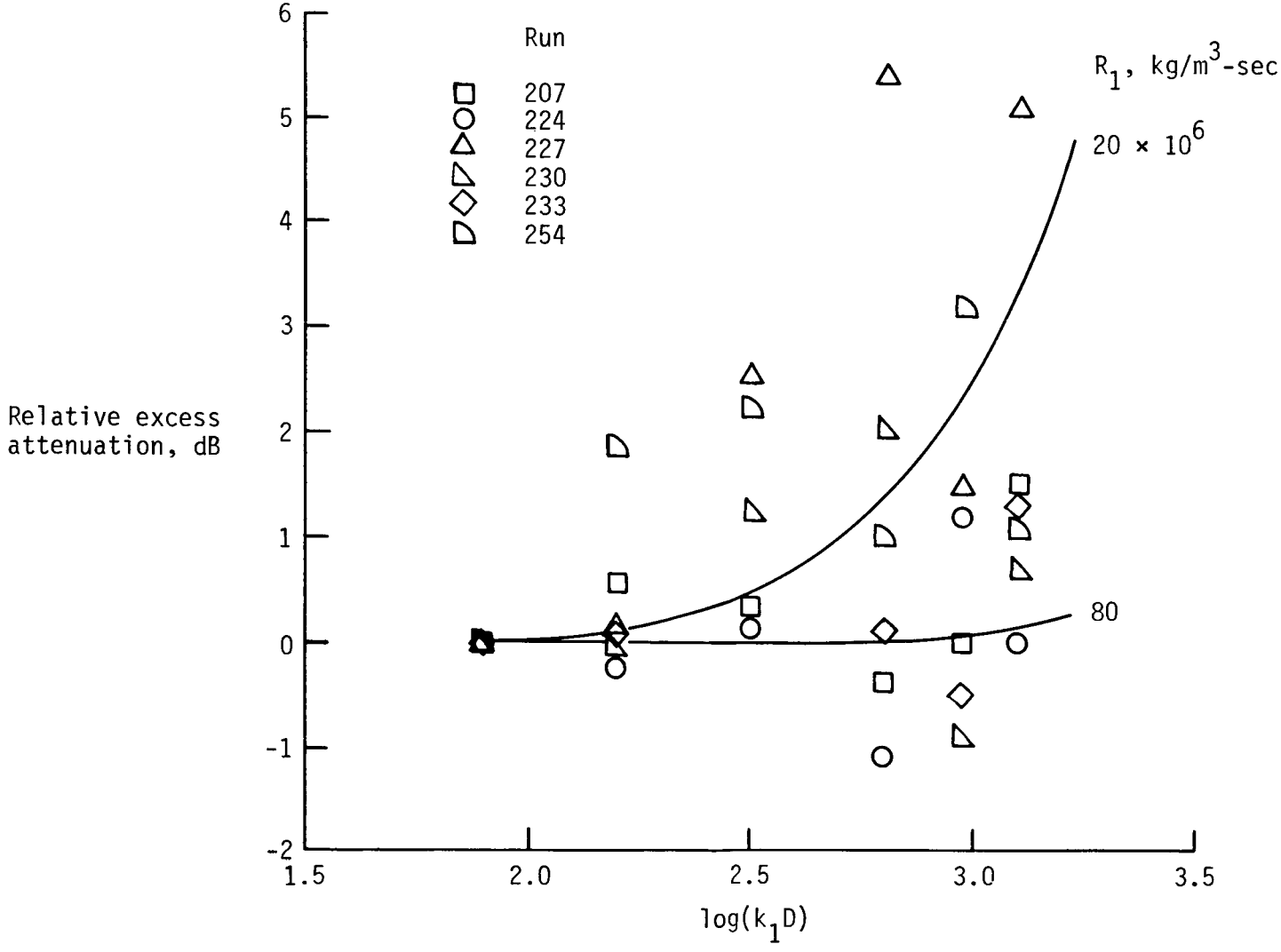

Figure 30. Comparison of measured and calculated relative excess attenuation for two values of R_1 at frequency of 12.5 kHz for hard surface with source and microphones at zero elevation.

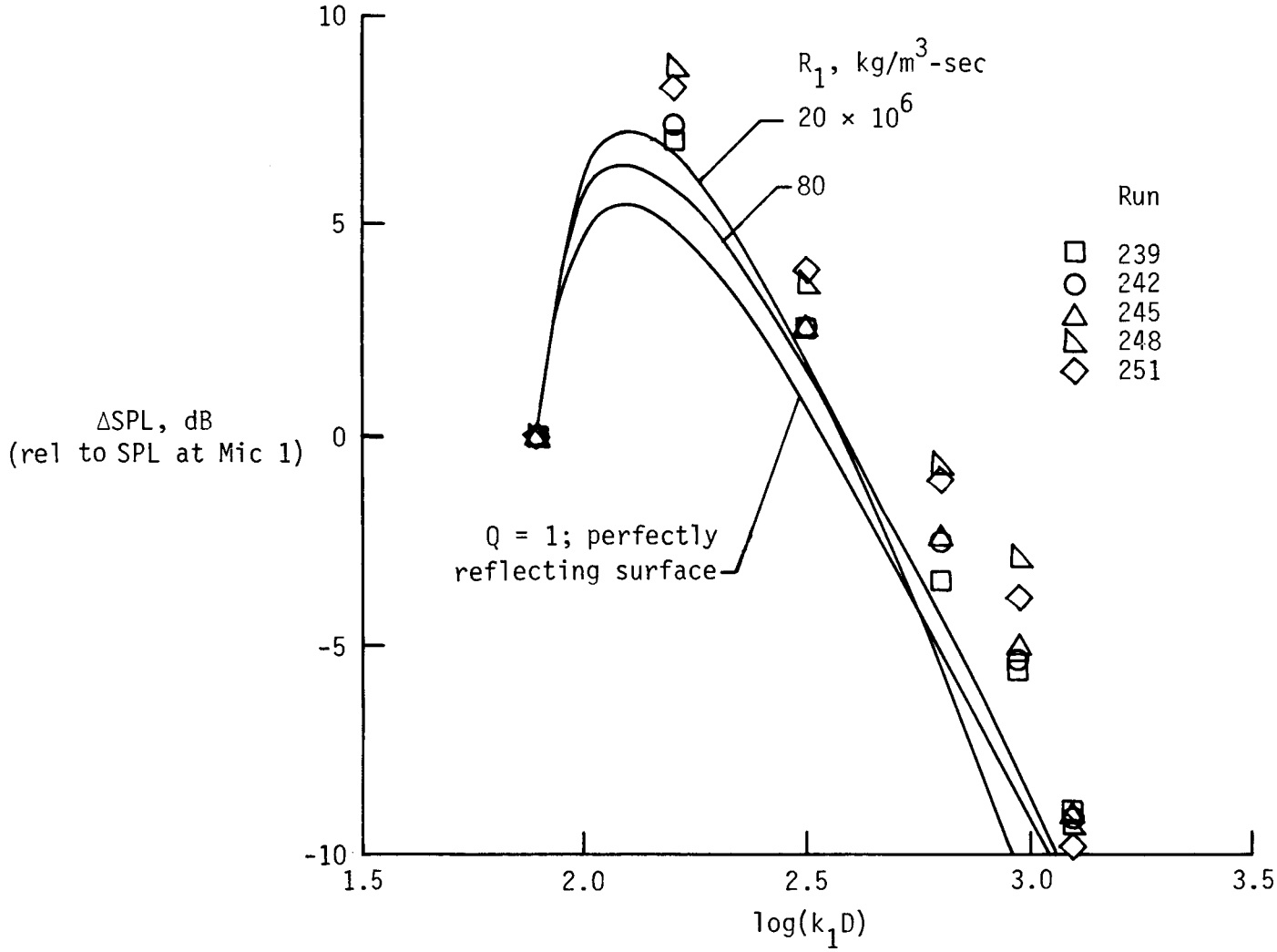

Figure 31. Comparison of measured and calculated changes in radial SPL distributions at frequency of 12.5 kHz for hard surface with source and microphones at elevations of 5.84 and 3.56 cm.

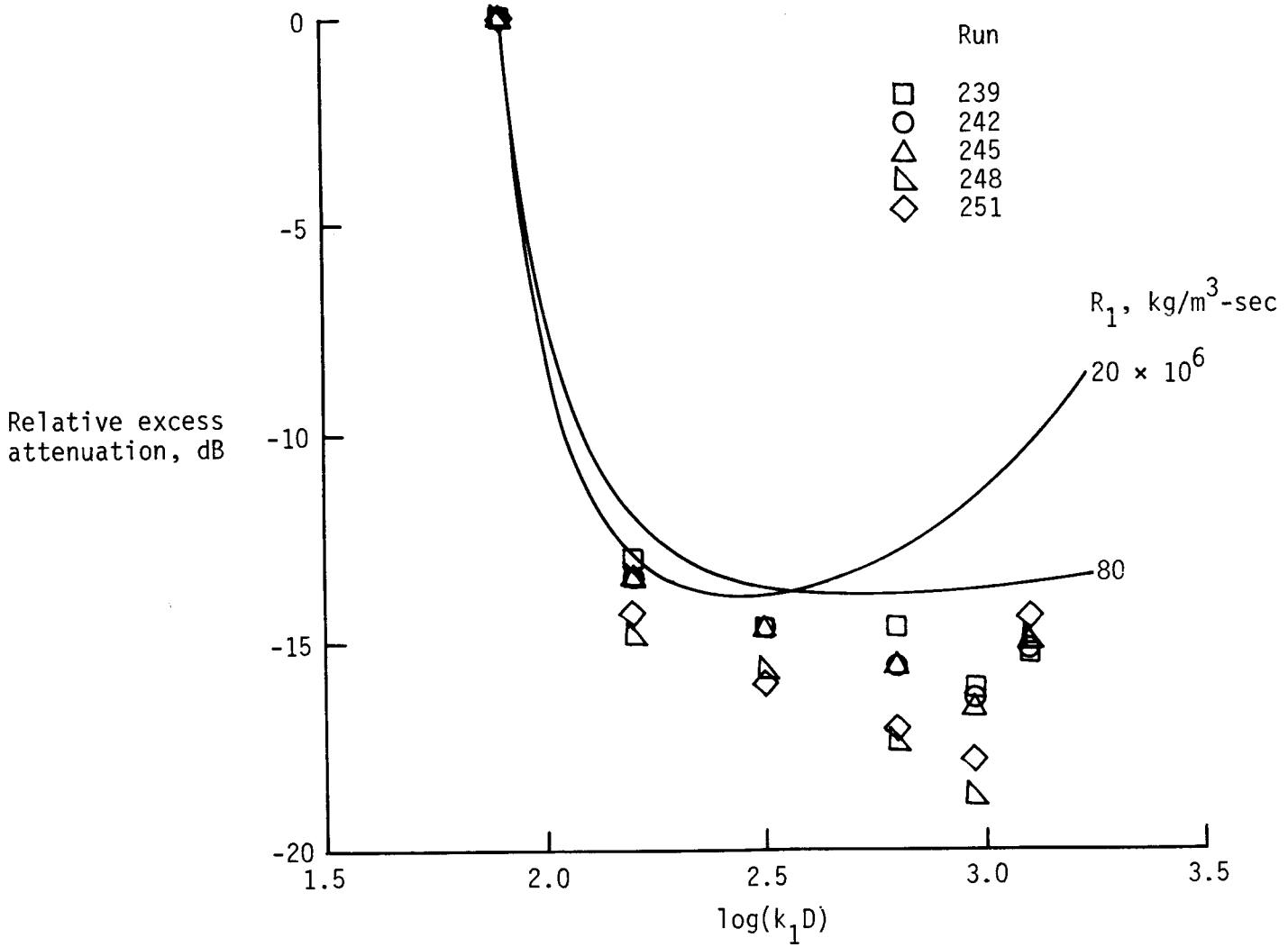

Figure 32. Comparison of measured and calculated relative excess attenuation for two values of R_1 at frequency of 12.5 kHz for hard surface with source and microphones at elevations of 5.84 and 3.56 cm.

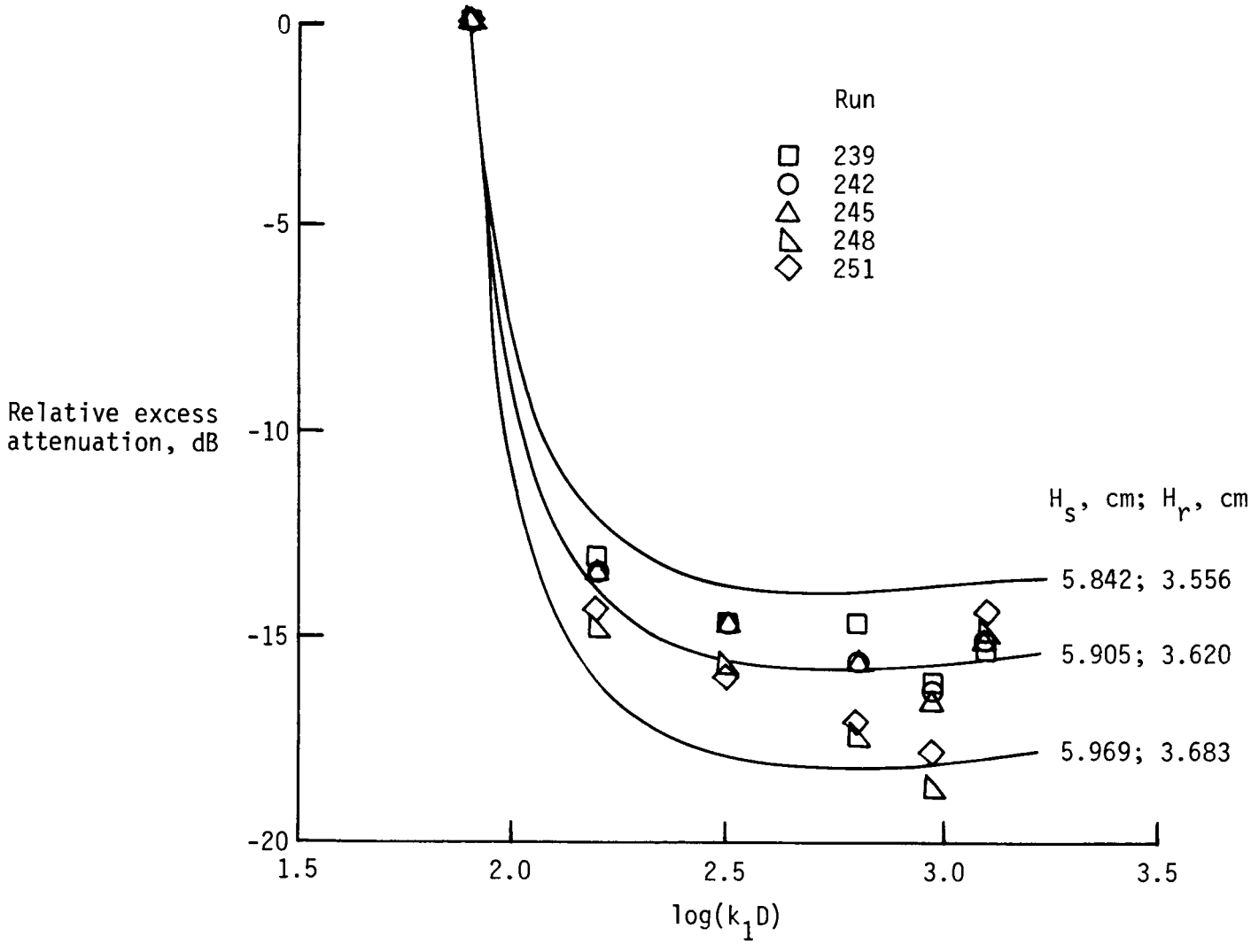

Figure 33. Comparison of measured and calculated relative excess attenuation for three source and microphone elevations at frequency of 12.5 kHz for hard surface.

NASA
National Aeronautics and Space Administration

Report Documentation Page

1. Report No.	2. Government Accession No.	3. Recipient's Catalog No.
NASA TP-2748		

4. Title and Subtitle	5. Report Date
Evaluation of a Scale-Model Experiment To Investigate Long-Range Acoustic Propagation	November 1987
	6. Performing Organization Code
7. Author(s)	8. Performing Organization Report No.
Tony L. Parrott, Gerry L. McAninch, and Ingrid A. Carlberg	L-16300
9. Performing Organization Name and Address	10. Work Unit No.
NASA Langley Research Center Hampton, VA 23665-5225	505-61-11-02
	11. Contract or Grant No.
12. Sponsoring Agency Name and Address	13. Type of Report and Period Covered
National Aeronautics and Space Administration Washington, DC 20546-0001	Technical Paper
	14. Sponsoring Agency Code

15. Supplementary Notes

16. Abstract

Tests were conducted to evaluate the feasibility of using a scale-model experiment situated in an anechoic facility to investigate long-range sound propagation over ground terrain. For a nominal scale factor of 100:1, attenuations along a linear array of six microphones colinear with a continuous-wave type of sound source were measured over a wavelength range from 10 to 160 for a nominal test frequency of 10 kHz. Most tests were made for a hard model surface (plywood), but limited tests were also made for a soft model surface (plywood with felt). For grazing-incidence propagation over the hard surface, measured and predicted attenuation trends were consistent for microphone locations out to between 40 and 80 wavelengths. Beyond 80 wavelengths, significant variability was observed that was caused by disturbances in the propagating medium. Also, there was evidence of extraneous propagation-path contributions to data irregularities at the more remote microphones. Sensitivity studies for the hard-surface model indicated a 2.5-dB change in "relative" excess attenuation for a systematic error in source and microphone elevations on the order of 1 mm. For the soft-surface model, no comparable sensitivity was found.

17. Key Words (Suggested by Authors(s))	18. Distribution Statement
Acoustic propagation Scale model Long range Grazing incidence Excess attenuation	Unclassified—Unlimited Subject Category 71

19. Security Classif.(of this report)	20. Security Classif.(of this page)	21. No. of Pages	22. Price
Unclassified	Unclassified	54	A04

For sale by the National Technical Information Service, Springfield, Virginia 22161-2171